LAPPEENRANTA UNIVERSITY OF TECHNOLOGY

School of Engineering Science

Double Degree Programme in Chemical and Process Engineering

MASTER'S THESIS

Rare-earth metals adsorption on a novel bisphosphonate separation material

Examiner: Prof. Tuomo Sainio

Supervisor: D.Sc. Sami Virolainen

Lappeenranta 13.7.2016

Lukina Liubov

Punkkerikatu 5 D64

53850 Lappeenranta Finland

Tel. +358 44 936 08 59

ABSTRACT

Lappeenranta University of Technology
Chemical Engineering Department
Double Degree Programme in Chemical and Process Engineering

Liubov Lukina

Rare-earth metals adsorption on a novel bisphosphonate separation material

Master's Thesis
2016
69 pages, 24 figures, 10 tables

Examiner: Prof. Tuomo Sainio
Supervisor: D.Sc. Sami Virolainen

Keywords: rare earth metals; adsorption; bisphosphonate; modeling, isotherms; separation material

Abstract

Rare earth metals are irreplaceable in many technological applications. In Europe, rare earths can be found in waste materials. Methods developed for rare earth metal separation and pre-concentration are not cost-effective. Adsorption is considered a simple and economical method for rare earth metals recovery. In this work, a novel bisphosponate-based adsorbent N10O was tested. The research objectives were to investigate performance of the adsorbent and to establish optimal conditions for recovery of Nd(III), Eu(III), Tb(III) from aqueous solutions.

Theoretical part of the work includes information on rare earth metals supply, demand and separation methods, as well as on properties of bisphosphonates and their use in metal chelation. In experimental part, batch adsorption in test-tube scale was used. The influence of pH, temperature, ionic strength, initial metal concentration and contact time on adsorption process were investigated from HCl, HNO_3 and H_2SO_4 media. Metal concentrations were subsequently analyzed by ICP-MS.

The experiments revealed that adsorption process was highly pH dependent. Optimal metal uptake in all three media was achieved after pH 2. The results also showed that the capacity of N10O was comparable to that of common ion exchange resins (>200 mg/g). Temperature proved to enhance the adsorption process. Selectivity coefficients for pairs of Nd, Eu and Tb turned out to be 1.2-2. Adsorption models were fitted to experimental data points. Langmuir-Freundlich isotherm shows the best fit. Empiric kinetic models suggest that adsorption process is controlled by film and intra-particle diffusion.

On the basis of the results of this research, it can be concluded that the adsorbent N10O is applicable for selective recovery of rare earth metals. Metal uptake is high in wide pH range and the capacity is similar to existing low-cost materials, or even higher. More experimental work is to be done for investigating kinetics and solubility of the adsorbent. For pilot-scale application, it would be beneficial to impregnate the N10O into carrier material.

ACKNOWLEDGEMENTS

At first, I would like to say that I really enjoyed writing and working on this thesis. It became a big and important part of my life.

First of all, to whom it may concern in Mining University of Saint Petersburg, LUT, and TekKem in particular – thank you to encouraging me into research path! I do hope that one day I will become a professional scientist and do something cool. This thesis will undoubtedly have contributed to it.

I owe my deepest gratitude to my supervisor D.Sc. Sami Virolainen, whose friendly advice and support was always appropriate. He was comfortable to work with, and his calm professional attitude encouraged me to perform at my best.

Professor Tuomo Sainio provided me with control and guidance in the right time, which was definitely very helpful.

I am grateful to Liisa Puro, who spent long hours with me in the ICP-MS room and assisted obtaining reliable results.

My father knows without me writing it here that we are one team, so my achievements are his achievements.

Moreover, I express my thanks to my friends Vitalii Kavun, Kirill Filianin and Anastasiia Selezneva, who distracted me from writing my thesis and laughed at my ICP-MS days, but also supported me all the time in Lappeenranta.

TABLE OF CONTENTS

LIST OF SYMBOLS AND ABBREVIATIONS - PART 1

BP(-s)	Bisphosphonate (-s)
IX	Ion exchange
OF	Objective function
REM, REE	Rare earth metal(-s), Rare earth element(-s): both used synonymously
SNE	Sum of normalized errors
α	initial adsorption rate, mg/(g·min)
$\alpha_{A/B}$	selectivity of separation A from B
a	desorption constant, g/mg
a_r	Redlich-Peterson isotherm constant, mg−1
a_s	Sips isotherm constant, $dm^3 \cdot mg^{-1}$
A_T	Temkin isotherm equilibrium binding constant, $dm^3 \cdot g^{-1}$
a_{Toth}	Toth isotherm constant, $dm^3 \cdot mg^{-1}$
b_R	Redlich-Peterson isotherm exponent
b_s	Sips isotherm exponent
b_T	Temkin isotherm constant
b_{Toth}	Toth isotherm exponent
C_0	initial concentration in liquid phase at t=0, mg· dm^{-3}
C_{aq}	amount of metal in aqueous solution, mg
C_{BP}	amount of metal adsorbed on the BP, mg
C_e, C_{eq}	metal ion concentration in the solution, mg· dm^{-3}
C_i	molar concentration of ion i, mol
C_t	concentration in liquid phase at time t, mg· dm^{-3}
D	distribution ratio of REM between liquid and solid phases
E%	extraction percent of metal ions, %
f_i	value of error function i (i=1…7)
f_{max}	maximal value of error function i in the row of j values
I	ionic strength, mol
k_1	pseudo-first-order rate constant, min^{-1}
k_2	pseudo-second-order rate constant, g/(mg·min)
k_{diff}	rate constant for intra-particle diffusion
kr_1	pseudo rate constant in step 1 for reaction 1.

LIST OF SYMBOLS AND ABBREVIATIONS - PART 2

kr_{-1}	pseudo rate constant in step 1 for reaction -1
k'_{r1}	rate constant in step 1 for reaction 1.
k'_{r-1}	rate constant in step 1 for reaction -1.
K_F	Freundlich isotherm constant
K_L	Langmuir isotherm constant, $dm^3 \cdot mg^{-1}$
K_R	Redlich-Peterson isotherm constant, $dm^3 \cdot g^{-1}$
K_s	Sips isotherm model constant, $dm^3 \cdot g^{-1}$
K_{Toth}	Toth isotherm constant, mg/g
m	partial order for adsorbate
$m_{adsorbent}$	dry adsorbent mass, g
n	partial order for adsorbent
n_e	number of experimental data points
n_f	adsorption intensity
p	number of parameters for given isotherm model (2 or 3)
q, q_t	solid phase concentration of metal ions at time t, $mg \cdot g^{-1}$
q_e, q_{eq}	solid phase concentration of metal ions at equilibrium, $mg \cdot g^{-1}$
q_{calc}	loading, calculated by models, $mg \cdot g^{-1}$
$q_{m,}$	Langmuir monolayer saturation capacity, $mg \cdot g^{-1}$
q_{max}	maximal loading, $mg \cdot g^{-1}$
q_{meas}	measured loading, $mg \cdot g^{-1}$;
R	Universal gas constant, 8.314 J/mol °K
R^2	Coefficient of determination, R squared
t	time, min
T	absolute temperature, °K
V_{sample}	volume of sample, l
z_i	charge numer of ion i

1. INTRODUCTION

1.1 Background

Rare earth elements are a group of 17 metals, including 15 lanthanides, yttrium and scandium. Demand for rare earths has surged in the past decade due to their importance in ecological and hi-tech applications. Wind turbines require strong magnets, as well as electric cars. For energy efficient lighting, REE-containing phosphors are needed. Military applications include missiles, fighter jets, sensors, guided munitions, electronic warfare. Health industry uses REM in medical imaging. Generally speaking, rare earth metals allow us to have fast, light, durable, high-performance ecological products, which is the key issue of modern world.

According to senior fellow of the Institute for the Analysis of Global Security Jack Lifton, there is no single rare earth element market, but several distinct "critical rare earth" markets. It is these critical metals which will remain scarce even with new mine supplies and extraction technologies. One of them is neodymium, which is widely used in permanent magnets. The other are heavy rare earth elements applied in various technological sectors, including europium, terbium, dysprosium and yttrium. Substitutions for rare earths metals are not nearly as efficient as genuine REM.

Currently China beholds 90% of world rare earth metal production, with Australia and United States of America being the second and third largest producers. Europe does not have any REM mines in use. Dependence on import of rare earths from a single source is an undesirable uncertainty for European Union.

Rare earth metals can be found in electronic scrap or mining waste. However, the concentrations of REM in waste materials are low, and for the time being, the extraction is not economically viable. New efficient ways to recover rare earth metals from waste materials are required. Among the other methods for rare earth metal separation, adsorption is considered promising.

In 2015, research group of Prof. Jouko Vepsäläinen from University of Eastern Finland discovered that a recently synthesized bisphosphonate adsorbent N10O can be successfully

applied for metal recovery from aqueous solutions. The question arises, whether this economic material can be used for selective rare earth metal separation of rare earth metals.

1.2 Research objectives

This study aims at assessment of applicability of the novel adsorbent for rare earths recovery from aqueous solutions. Three critical rare earth metals are reviewed, namely Nd, Eu, Tb. Main objectives of this research are:

1. To find optimal parameters for separation process;
2. To obtain fundamental data on adsorption;
3. To investigate selectivity of adsorption.

1.3 Research structure

In order to achieve the research objectives, both theoretical and practical work was done. To obtain data on adsorption process and to find optimal parameters of adsorption, experiments with different temperature, pH, ionic strength and time were conducted.

Theoretical basis was established after review of literature sources, which can be found in the Section 9 “References”. Experimental results were compared with literature data, when it was appropriate. In this study, batch adsorption in test-tubes was performed. Metal concentrations were analyzed by ICP-MS. More detailed description of materials and techniques used can be found in the Section 6 “Experimental”. All the practical work for this thesis was done in the laboratories of LUT Kemia, Lappeenranta University of Technology, Finland.

Theoretical part of this thesis covers general information about rare earth metals, bisphosphonates and existing methods for rare earth metals separation and purification. Moreover, equations and models which were applied for interpretation of experimental data, are cited. Practical part describes the results of the experiments, which are then analyzed in the Section 7 “Results and discussion”. Overall summary of the work is given in the end.

2. RARE EARTH METALS

2.1 Properties and applications of rare earth metals

All rare earth metals can be divided into two groups: light rare earth elements (LREE) and heavy rare earth elements (HREE). This division is based on electronic configuration of metal atoms. LREE including the row La – Gd have just single clockwise-spinning electrons on the outer shell, whereas HREE from Tb to Lu have paired electrons. Yttrium is in the HREE group, but Sc belongs to neither group, based on ionic radius and chemical properties. REE are rather abundant in earth crust, although not concentrated, which makes them difficult to extract and separate from each other. This feature is the reason why rare earth metals are so called. The word "rare" is used in the old sense here, meaning "difficult".

In this work, three critical rare earth metals are reviewed: neodymium, europium (both LREE) and terbium (HREE). Applications only for these elements are therefore cited.

Neodymium is a soft silvery metal with oxidation state +3 which tarnishes in air. It was first discovered in 1885 by Austrian scientist Carl Auer von Welsbach. Main minerals containing Nd are bastnäsite and monazite. It does not exist as a single metal, and generally the refinery is needed to extract Nd from a mixture of lanthanides. Nd is widely distributed in the Earth crust, with a concentration $\sim 4 \cdot 10^{-5}$ kg/kg (Wedepohl 1995) with abundance similar to Co, Ni and Cu.

Chemicals with Nd first appeared as glass additives in 1927 and still are used for this purpose. Neodymium is also applied in solid-state lasers. Another popular application is producing alloys for powerful magnets, which are used in audio, video devices, as well as in hard disks. Efficient low-weight electric motors for hybrid cars and generators for aircraft and wind turbines also use Nd magnets.

Europium was discovered in 1896 by French chemist Eugène-Antole Demarçay. It is a hard silvery metal prone to quick oxidizing in water and ambient air. It has oxidation states +2 and +3. Commercial applications if Eu are less numerous than for other REM: it is mostly used in glass and lasers as dopant. Its phosphorescence is used as well in light

bulbs, anti-forgery banknote marks and TV and computer screens. Europium constitutes ~$2 \cdot 10^{-6}$ kg/kg of Earth crust, essential sources being monazite, xenotime, loparite and bastnäsite (Wedepohl 1995). Content of Eu in deposits is usually low (0.2% for biggest REE mine Bayan Obo in China).

Terbium is a silvery-white metal, soft enough to be cut with a knife. Together with many other REM, it was found in the mine if Ytterby, Sweden. As a separate element it was discovered in 1843 by Swedish chemist Carl Gustaf Mosander. Terbium is a component of many minerals such as cerite, gadolinite, monazite, xenotime and euxenite, with abundance in Earth crust of ~4·10-5 kg/kg (Wedepohl 1995).

Applications of Tb include dopants for materials constituent solid-state devices, crystal stabilizers for high-temperature fuel cells and components of Terfenol-D, magnetostrictive material. Green phosphors, TV tubes and fluorescent lamps employ terbium oxides.

Similar to other lanthanides, neodymium, europium and terbium do not show particularly high toxicity. Toxicity was examined for female rats, and LD_{50} turned out to be 2750 mg/kg for Nd, and >5000 mg/kg for Eu and Tb (Bruce et al. 1963).

2.2 Rare earth metals production

Over 90% of REE are found in primary or byproduct placer deposits such as alluvial sands on beaches or along the riverbeds. Frequently occurring minerals containing REE are monazite (REE)PO_4, bastnäsite (REE)CO_3F and xenotime (REE)PO_4 (Beauford 2010). Lighter elements are more abundant and make for 80-99 % of total deposit. Main source of LREE is monazite, and xenotime chiefly incorporates HREE. In any rare-earth mineral the elements of even atomic number are more abundant than those of odd. Rare earths can be found in clay deposits, where the elements are adsorbed onto the clay particles. This source comprises a small percent of the total REE market, yet it is important because it provides some of the HREEs (Terry 2011). Quite often REE occur in a form of byproduct of mining and processing Cu, Au, U, phosphates.

First rare earth ores were found in Sweden, in 1787. Industrial use of REM began only after a century. First producers of rare earths were Brazil and India. Australia and Malaysia joined exporting REM in 1940s. United States of America started extracting REM from the

Mountain Pass Mine, and by 1960 they have become leading producer of rare earths. However, in 1980s China entered the game and quickly achieved the dominating place in the world REE production. Crushed by low-cost rare earths from China, other countries soon closed their mines. Only around the beginning of 21st century rare earth producers understood that Chinese monopoly is taking place, and since then production was restarted in the U.S., Australia, Malaysia and other countries. Biggest U.S. rare earth mining company Molycorp, previously the world leader, was on the second place in rare earth mining industry during the last decade. However, it is not easy to confront China, and in January 2016 Molycorp filed for bankruptcy protection.

In general, bastnäsite deposits in China and the US make up the largest part of the world's REM resources. China also faces some problems concerning REM industry: production stoppages, overproduction and illegal business. However, as can be seen in the table 1, in 2015 Chinese REM production constituted 85 % of total world production. Even taking into account significant drop from 2010, China still controls most of the REM market. Second largest source after bastnäsite is monazite, which is mined in Australia, Brazil, China, India, and Malaysia. In the table 1 below world mine production and reserves is shown (U.S. Geological Survey 2016).

Table 1 – World mine production of REE

Country	Mine production 2014 [t]	Mine production 2015 [t]	Reserves [t]
United States	5400	4100	1800000
Australia	8000	10000	3200000
Brazil	0	0	22000000
China	105000	105000	55000000
India	NA	NA	3100000
Malaysia	240	200	30000
Russia	2500	2500	NA
Thailand	2100	2000	NA
Other countries	NA	NA	41000000
World total	123000	124000	130000000

Europe does not have any REM mines in use. The project ERECON has identified rare earth deposits for further study in Sweden, Finland, Greece, Spain, Greenland, Norway, and Turkey (ERECON 2015). Of particular importance for their REE potential are deposits

in Greenland, Gardar province and Sweden, Norra Kärr. Figure 1 provides an overview of major REE locations in Europe.

Theoretically, REM recovery from electronic waste, old mines and other waste materials is one of the best options (Gutfleisch et al. 2011). Moreover, there already exist rare earth recycling companies, such as La Rochelle in France, Treibacher AG in Austria, Silmet in Estonia and Less Common Metals in UK. But in reality, less than 1 % of rare earth containing wastes is recovered. This is due to limitations in flowsheet design, inefficient collection rates and lack of information on REM content (Binnemans et al. 2013).

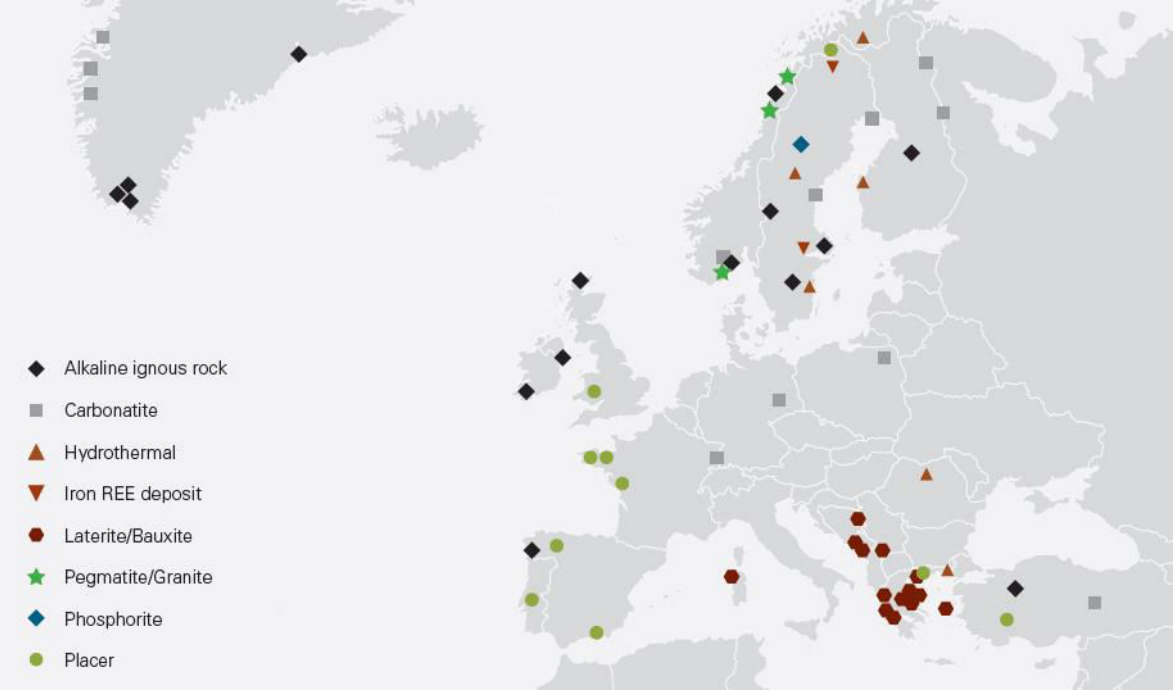

Figure 1 – Overview of major REM sources in Europe (ERECON 2015)

2.3 Rare earth metals demand

Rare earth elements are indispensable because they are involved in many hi-tech devices used in green energy, defense, electronics. According to report “Commodities at a glance - special issue on rare earths” (SUC 2014), the global demand in REM in 2015 was as shown on a Figure 2 below. According to data from ERECON (2015), REE demand, which was constant through the years 2006-2014, is going to increase by more than 20% compared to 2014 level by 2017. By 2020 it could be 50% higher than in 2014. This is due to growing R&D in green technologies and other application areas of rare earths.

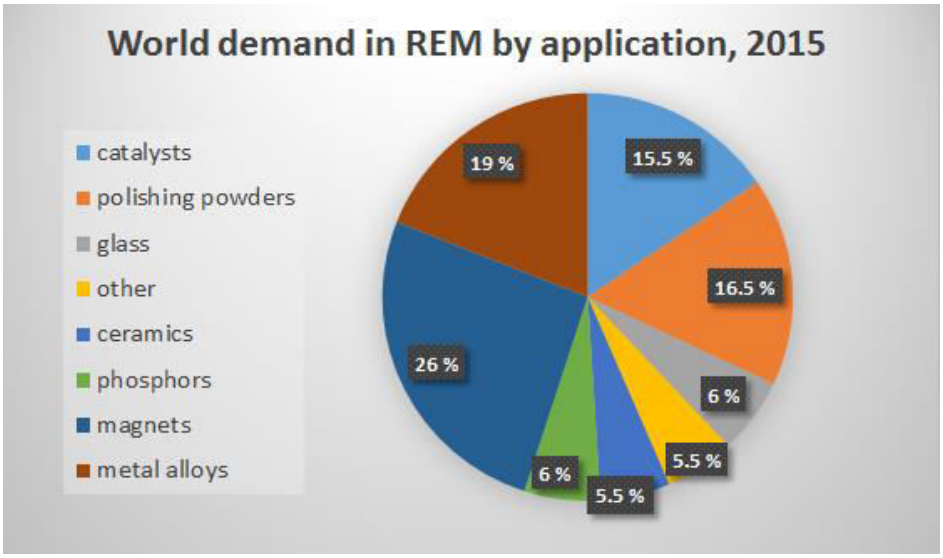

Figure 2 – World REM demand (SUC 2014)

Substitutions may mitigate scarcity of supplies, but do not resolve the problem completely. Light emitting diodes, batteries and solid-state drives are currently reducing use of REM in corresponding applications. Research is made with aim to decrease need in REE for permanent magnets. It is especially important for carmakers, who try to get rid of rare earths in fear of future supply disruption. Still, for many technologies rare earths remain essential and more applications for REM can emerge in near future. Figure 3 below represents substitutability of REM taken as a group. It can be well seen that most of rare earths do not have good cheap substitution materials. (CRM_InnoNet 2016).

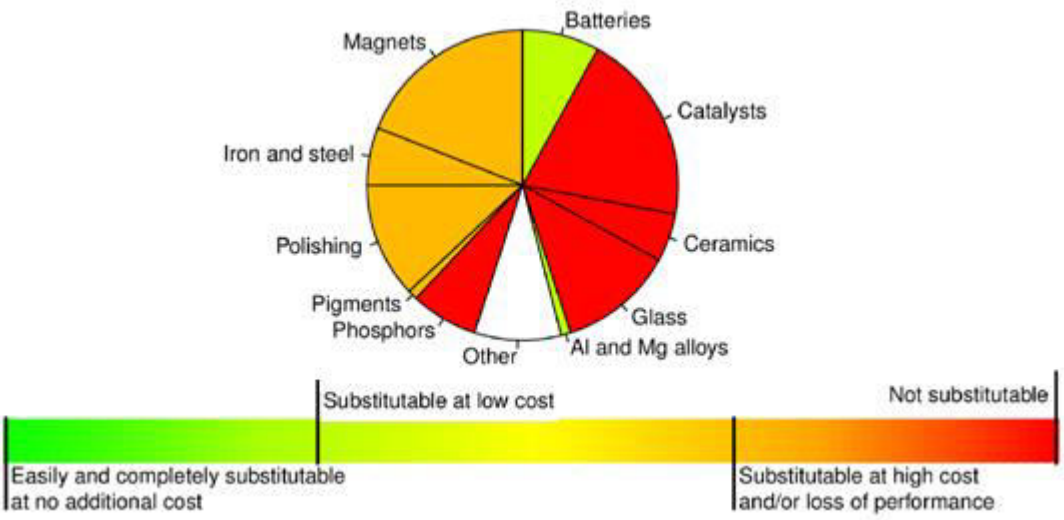

Figure 3 – Substitutability assessment (CRM_InnoNet 2016)

3. BISPHOSPHONATES

3.1 Properties of bisphosphonates

Currently the bisphosphonates (BP) are mostly applied for medical purposes. Therefore, not much scientific research is done to investigate BP applicability for wastewater treatment or valuable metals extraction.

Due to unmanageable amount of materials consecrated to bisphosphonates in general, this literature review will cover general information about the bisphosphonates and focus on what is essential for the topic of the thesis: metal chelation with bisphosphonates.

First introduction of bisphosphonates was done in 1865 by Nikolay Menshutkin, Russian scientist from Saint Petersburg State University. In the years that followed the discovery of bisphosphonates, these chemicals were used to prevent corrosion and scaling. They were also applied in the textile, oil and fertilizer production. Nowadays the main use of BPs lies in medical science, in the field of bone-related diseases.

The name “bisphosphonates” originates from the presence of two phosphonate groups. Bisphosphonates are chemically stable molecules containing O=P-C-P=O structure, so-called P-C-P "backbone" (Figure 4, left). The long alkyl side chain and short side chain determine chemical properties, mode of action and strength of bisphosphonate medicines. The structure of the BPs allows innumerable variations, each leading to different solubility, affinity to metals, efficacy etc. This makes the group of bisphosphonates very promising for a number of applications and for further scientific research.

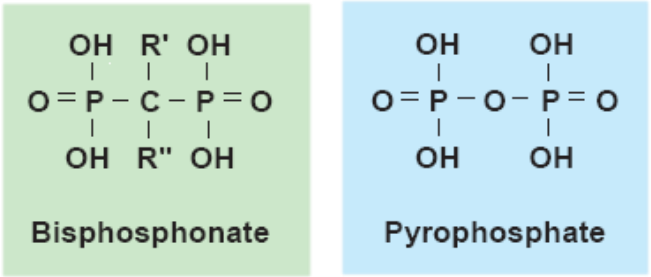

Figure 4 – Bisphosphonate and pyrophosphate molecule

If the two C-P bonds are located on the same carbon atom the compounds are called geminal bisphosphonates (although usually just bisphosphonates), and they are analogs of pyrophosphate (Figure 4, right) that contain an oxygen atom instead of a carbon.

Pyrophosphate bears a function of inhibiting excess calcification. A bisphosphonate group mimics pyrophosphate structure, thereby stopping activation of enzymes that utilize pyrophosphate and preventing bone resorption. (Alanne 2014). Human disorders where bone resorption takes place are commonly found and include osteoporosis, cancer, Paget's disease.

The mechanism of action of the BPs in the body is interesting for this thesis, because it bases on metal chelation. Due to complexing ability of O=P-C-P=O moiety, BPs can chelate metal ions, such as Ca^{2+}. And the hydroxyapatite in our bones is made mostly of $Ca_3(PO_4)_2$. When bone resorption occurs, special bone cells osteoclasts start breaking bone tissue in order to release calcium to the blood. At this moment, bound bisphosphonate is released from bone surface to the environment and is transported inside the bone-breaking cells. This inhibits action of bone-breaking cells or causes their death. On the other hand, the bisphosphonates also enhance activity of bone-building cells, osteoblasts. Therefore the bisphosphonates can effectively treat and prevent cases when bone mass is lost.

Ten bisphosphonates are commercially available and mostly used today for treatment of bone disease. Moreover, bisphosphonates can contribute to cancer treatment (Gnant & Clezardin 2012, Morgan & Lipton 2010), inhibit parasitic protozoa (Ghosh et al. 2004) and help with inflammatory joint diseases (Iannitti et al. 2012). Generally, the bisphosphonates are divided into 2 groups based on their structure and action mode: non-nitrogen containing BPs and nitrogen-containing BPs. The N10O, which is under review of this thesis, contains amino group, which reflects strongly its ability to chelate metals (Matczak-Jon 2010).

The ability of bisphosphonates to chelate metal ions is fundamental for all non-medical applications of BP's. Bisphosphonates have been studied for metal uptake from aqueous solutions (Alanne 2014). Moreover, potential of multilayer thin films involving BP and metal ions was investigated by Neff et al (2000) for possible application in semiconductor

technologies. Microporous bisphosphonate metal complexes present yet another probable application. Such materials react by all the mass instead of just surface layer, which can be employed in catalysts, sensors and chemical separations (Lohse & Sevov 1997, Neff et al. 2000). Summary of all medical and non-medical applications of the bisphosphonates can be found in Table 2.

Table 2 – Summary of applications of bisphosphonates (Alanne 2014)

Non-medical applications	Medical applications
1. Metal removal from water solutions 2. Thin films – Semiconsuctor industry 3. Microporous materials – Molecular sieves – Catalysts – Ion exchangers – Sensors 4. Plant impact – Enhancement of plant growth – Herbicidal effect	1. Inhibition of bone resorption 2. Antiparasitic effects 3. Anticancer effects 4. Bone targeting 5. Anti-inflammatory effects

3.2 Metal chelation with bisphosphonates

Complexation of bisphosphonates with various metals was extensively studied. For instance, complexation ability of bisphosphonates towards Cu^{2+}, Fe^{3+} and Al^{3+} was put in evidence. (Gumienna-Kontecka, 2002a; Gumienna-Kontecka, 2002b).

Complex-forming properties of diphosphonic acid derivatives with zinc(II), magnesium(II) and calcium(II) were investigated (Matczak-Jon 2010). Stabilities for complexes formed by transition and alkaline-earth metals were defined for complexons based on aminodiphosphonic acid. (Matveev, 1998). Modified bisphosphonates were also used to synthesize complexes with manganese, cobalt and copper (Kunnas-Hiltunen et al. 2010).

Bisphosphonates were used as solvent extraction reagents for actinides and Fe(III) (Chiarizia et al. 2001). Moreover, bisphosphonate sequestering agents for uranium(VI) chelation were evaluated (Sawicki 2008). Biomass-based adsorbent featuring bisphosphonate was

able to chelate Au^{3+} ions, as shown by Yin et al (2013). Multifunctional chelating ion exchange resin Diphonix® was created based on geminally substituted diphosphonic acid ligands chemically bonded to a styrene-based polymeric matrix (Chiarizia et al. 1997). Similar approach was employed for making a resin Dipex, which is suitable for chromatographic separations of actinides (Horwitz et al. 1997).

Rare earth metal chelation with bisphosphonates is less covered in literature, compared to chelation of actinides or other more common metals. Europium(III) complexes with diphosphonic acid were prepared, together with copper(II), iron(III), thorium(IV) and uranium(VI) (Herlinger et al. 1996). In addition, actinide and europium coordination complexes with ligands bearing phosphonate groups were examined (Nash 1997). Complexes formed between Sm^{3+} and the bisphosphonate ligand pamidronate in aqueous solution were investigated (Arabieh 2015). Coordination polymer platform has been prepared from zirconium (IV)-bisphosphonate in order to extract Th(IV) and lanthanides from acid solutions (Luca 2015).

3.3 Novel bisphosphonate N10O

In 2012, ten aminobisphosphonates were synthesized by research group of University of Eastern Finland (Alanne 2014). Among them, the BP with chain length of 10 and with the formula as shown on the Figure 5, was created.

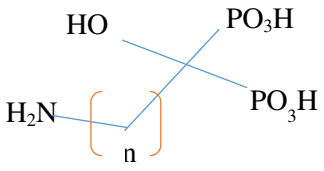

Figure 5 – Structure of the recently synthesized BP named N10O (Alanne 2014)

Instead of chemical name 11-amino-1-hydroxyundecylidene-1,1-bisphosphonic acid, the shorter version is used for reference to this novel material. The name N10O indicates that the length of carbon chain is 10 and that nitrogen is incorporated at one of the side chains.

The N10O was kindly provided by UEF in a form of white thin powder. The average size of flake-resembling crystals was found to be 2 x 30 x 50 μm. Due to the length of the carbon backbone, the material practically does not dissolve in water, the solubility being 59 mg/l, as shown by experiments Nitrogen BET surface area was found to be 11.4 m2/g. (Alanne 2014).

Bisphosphonate N10O has microcrystalline structure that can adsorb metal cations due to its hydroxyl group and two geminally bound phosphonic acid groups. Each of such groups provides 1–3 donor oxygen atoms. They are used as hooks and bridging sites for metals in ionic form. After chelation, energetically favourable six-membered rings are formed. Amino group is not likely to participate in chelation. This BP shows high efficiency in collecting metal cations without additional resin or prior precipitation steps. It is easy and economic in terms of preparation and does not exert toxic effects. Loaded N10O can be recycled more than 20 times. Selectivity of extraction can be adjusted by changing pH and temperature, as well as by changing PCP-chain, characteristic structure of all bisphosphonates. This process is reported to be rather fast (<10 min or, in some cases, less than 1 min) and high-performant even with low metal concentrations. (Turhanen et al. 2015).

The N10O was tested for chelation of alkali and alkaline earth elements. It turned out, that Li, Na, K and Cs are not efficiently chelated, whereas Cr, Fe, Co, Ni, Zn, Cu were bound in a wide pH region. Highly acidic conditions cause binding sites protonation, so the collection in the most cases occurred after a certain pH value. The capacities for different metals varied from 5 to 78 mg/g. (Ibid).

4. RARE EARTH METAL SEPARATION

4.1 Overview of separation methods

Separation and pre-concentration of lanthanides is one of the most difficult tasks if inorganic chemistry, due to small differences between physical and chemical properties of REM. Ever-increasing number of rare earth applications leads to deep interest in new sources and techniques for rare earth separation (Gupta 1992).

Hydrometallurgical methods offer lower energy consumption, air pollution and capital costs, when compared to pyrometallurgy. It also allows for processing of complex and low grade raw materials and constant control of emissions. (Virolainen 2016).

Generally hydrometallurgical treatment comprises the following steps: pre-treatment, aiming at improving metal dissolution; leaching; concentration and/or purification; recovery of metals from leach solution. For the purpose of this work, final step of the sequence, i.e. most common procedures for rare earth metal recovery from aqueous solutions will be reviewed.

Selective separation of rare earths was a classical problem in chemistry for many years. The complexity of it descends from the fact that all lanthanides have similar chemical properties, and rare earth minerals always contain REM mixture. All the separation methods invariably utilize slight difference in basicity resulting from ionic radius decrease from La to Lu (Moeller 1945). These differences impact solubility of salts, ion hydrolysis, complex formation which are employed in separation processes by fractional crystallization, solvent extraction, ion exchange, fractional precipitation. Notable fact is that property difference between rare earths decreases as the atomic number increases. In water solutions, lanthanides elements are normally trivalent, the exceptions being additional Ce^{+4}, Pr^{+4}, Tb^{+4} and low stability divalent ions: Sm^{+2}, Eu^{+2}, Yb^{+2}. Effective separation uses selective reduction/oxidation of these elements because different states show significant changes in behavior. (Gupta 1992).

The most abundant rare earth, cerium, can be separated relatively easily and early in the separation sequence by oxidation. This simplifies subsequent separation of the less abun-

dant rare earths. Samarium, europium, and ytterbium can easily be separated after reducing them to the divalent state. Unlike cerium, these elements are much less abundant and separation using reduction is carried out only after they are enriched by other procedures. (Ibid).

More than half a dozen different salts and double salts have been used for the separation of rare earth elements by fractional crystallization. This method has been considered to be the best of the classical separation procedures for producing the individual elements in high purity. However, LREE are more amenable to fractional separation than HREE. Due to smaller differences between adjacent elements, separation of REM from Sm and elements further to the right becomes cumbersome (Topp 1964).

As with fractional crystallization, a number of compounds have been studied for the separation of rare earths by fractional precipitation. The hydroxides and double sulphates, in particular, have been widely used. Different sulphates solubility allows to crudely separate mixture of REM into three groups. (Ibid).

Before 1947, the methods above were the only available for REM separation. They were inefficient, gave purity up to 99,9 % (3N) and required considerable time and effort. Starting from 1950s, techniques of ion exchange and solvent extraction have dominated field of rare earths separation. Also oxidation/reduction techniques are effectively applied for separation of single REE from mixture of rare earths in case of Ce and Eu (Zhang et al. 2016).

Ion exchange is used to separate and produce rare earth products with purity up to 7 N but capacity and efficiency of this method are low. Therefore it is just used to obtain small amount of high purity product for electronics or analysis (Xie et al 2014).

Solvent extraction methods are most widely applied for separation of REM since 1990s (Zhang et al. 2016). As extractants, cation and anion exchangers are used, as well as solvation extractants and chelation agents (Xie et al. 2014). The choice of extractant depends on selectivity and hydrometallurgical solution properties. Commercial products D2EHPA, HEHEHP, Versatic 10, TBP, and Aliquat 336 are widely used in rare earth industry (Xie et al. 2014).

Solvent extraction method also has limitations. Firstly, big volumes of organic solvents are needed, and consequently big amounts of wastewaters are formed. Moreover, the process is very time-consuming and difficult to automate (Svard 2015). To perform a target purity level, up to hundred stages of mixing and settling equipment can be installed.

4.2 Sorption of rare earth metals

As shown above, there are many methods for separation, purification and pre-concentration of rare earths. However, these methods are not attractive from economical point of view (Anastopoulos et al. 2016). On the contrary, adsorption has gained attention as possible way to recover REM in efficient, simple and rather inexpensive manner using low-cost materials. Importance of adsorption due to its simplicity, wide ranging applicability and possibility to use even with low rare earth concentrations was shown in a number of publications. (Diniz & Volesky 2005; Ogata et al. 2015; Ogata et al. 2016; Zhao 2016; Gładysz-Płaska et al. 2014 etc.).

In the process of ion exchange separation or REE, polystyrene-sulphonic cation exchangers are used. As they do not differ in affinity towards rare earth metals, elution technique with complexing agent is used. The main disadvantage of such method is that there is no universally selective eluent for all the rare earths. Anion exchange was applied significantly lower than cation exchange, due to more complex sorption mechanism (Kolodynska & Hubicki 2012). Strong anion exchange resins do not work in mineral acids, but decent adsorption occurs in other media. Among others, Dowex, Amberlite, Purolite ion exchangers were successfully applied for separation of rare earths.

In contrast to cation and anion exchange resins, chelating ion exchange resins have different affinity towards rare earth elements. The chelation capacity depends on the functional groups and pH. According to Kolodynska & Hubicki (2012), phosphonic, phosphate, phosphinic, iminodiacetate and other functional groups are used. Aminophosphonic ion exchange resins are of particular interest for this work, such as BP-based resins Dipex and Diphonix.

It would be interesting to compare the capacity of the common ion exchange resin with the capacity of the novel bisphosphonate. However, many studies do not determine the capacities for all rare earths. Moreover, experimental conditions vary for each case. The dry resin capacities of some ion exchangers which are successfully used for REM separation are shown in the Table 3.

Table 3 – Capacities of some IX resins used for REM separation

Resin	Dry capacity	Source
Dowex-50	5eq/g	Shubert 1949
Purolite C150TLH	1.8 eg/g	Purolite C150TLH Information brochure
Diphonix	5 meq/g	Kolodynska & Hubicki 2012
Dipex	1 meq/g	Horwitz et al. 1997

Recently, adsorption has gained significant attention as a cost-effective and eco-friendly solution to rare-earth metal recovery (Das 2013). Many natural materials were used for adsorption of rare earths, for example: granular hydrogel composite (Zhu & Zheng 2015); carbonized polydopamine nano carbon shells (Xiaoqi et al. 2016); modified red clays (Gładysz-Płaska et al. 2014) cysteine-functionalized chitosan magnetic nano-based particles (Galhoum et al. 2015).

After detailed screening of literature, big quantity of publications was found, dealing with various low-cost adsorbents for removal or pre-concentration of different rare earth metals. On the contrary, there were virtually no references on rare earth metal recovery with the help of materials similar to bisphosphonates. Therefore, a decision was made to describe here the most recent data (≤ 3 years old) referring to progress in adsorption of the rare earths studied in this work.

For Nd, Eu and Tb, various adsorbents have been investigated since the year 2013. Information about them is summarized below. Adsorption capacities for the reviewed adsorbents are presented in the Table 4 in the end of this section.

Malt spent rootlets were reported to show the highest adsorption at pH 4.5, which was also the higher limit of the investigated pH range. Removal of Eu^{3+} was fast, equalling 60 min. (Anagnostopoulos et al. 2016).

Cactus fibres with various modifications were explored for Eu^{3+} removal. Maximum capacity was reached at pH 4 for raw fibres, and at pH 6 for modified materials. Adsorption process was found to be of chemical nature. (Prodromou & Pashalidis 2016).

Hydroxyapatite adsorbed Eu^{3+} ions in 30 min time, and intra particle diffusion was found to be a time determining step. Adsorption was of multilayer cooperative type. (Granados-Correa et al. 2013). Magnetic nano-hydroxyapatite adsorbed maximum Nd^{3+} at pH 5, main mechanisms being chemisorption and ion exchange (Gok 2014).

Adsorption by crab shells and chitosan nanoparticles removed Eu^{3+} rather quickly, reaching equilibrium after 60 min. Intra particle diffusion turned out to be not the only time determining step. Maximum adsorption was reached at pH 3. (Cadogan et al. 2014). Roosen and Binnemans (2014) showed that simple chitosan has low capacity for Nd(III), but EDTA-chitosan has a capacity of 74.4 mg/g.

Raw graphene oxide showed higher capacity than sulfonated graphene oxide, probably due to existence of two more oxygen functional groups. Maximum adsorption was obtained at pH 9, maybe the reason for it was precipitation of Eu^{3+} as $Eu(OH)_3$. Adsorption mechanism was explained by formation of two inner-sphere surface complexes. (Yao et al. 2016).

Magnetic composites with Fe_3O_4 and cyclodextrin showed better adsorption capacity for Eu^{3+} than simple Fe_3O_4. At low pH the adsorption mechanism was inner-sphere complexation. At higher pH adsorption was governed by inner-sphere complexation combined with precipitation. Equilibrium was achieved after 180 min. (Guo et al. 2015).

Adsorption of Eu^{3+} on mesoporous silicas of Santa Barbara Amorphous type SBA-15 functionalized with N-propyl salicylaldimine (SBA/SA) and ethylenediaminepropylesalicylaldimine (SBA/EnSA) was examined. Optimum condition for the process was obtained at pH 4. Increase of ionic strength did not impact the adsorption efficiency. Adsorption mechanism was explained as inner-sphere complexation of chemical nature. (Dolyatyari et al. 2016).

Maximum adsorption by silica-based urea-formaldehyde composite was noted at pH 6 for Nd^{3+} and Eu^{3+} after 120 min of equilibration. Impregnation with organophosphorous ex-

tractant and increasing temperature enhanced the adsorption. The process of sorption was controlled by intra particle diffusion. (Naser et al. 2015).

Calcium alginate and calcium alginate-poly glutamic acid hybrid gels were studied for the adsorption of Nd^{3+}. Equilibrium for both cases was reached after 6 hours. Modified material showed higher adsorption capacity than non-modified variant. (Wang et al. 2014).

Alginate-silica microspheres were designed for serving as stationary phase in chromatographic columns. This new material showed stable porous structure and higher resistance to acidic conditions (Roosen et al. 2015).

The solid-phase extraction procedure with natural Transcarpathian clinoptilolite thermally activated at 350 °C was used to pre-concentrate trace amounts of Tb^{3+} in aqueous solutions. Maximum sorption capacity towards terbium was observed at pH 8.25, and recovery varied from 93.3% to 102.0%. (Vasylechko et al. 2015).

Terbium (III) ions adsorption on 1-acryloyl-3-phenyl thiourea-based pH-sensitive hydrogel was examined by batch experiments studies. Optimum adsorption was noted at pH 7, with a little decrease in adsorption at pH 9 and 10.The kinetic study showed that the pseudo-second order model was appropriate to describe the adsorption mechanism (Reddy et al. 2016).

Hydroxyapatite surface was modified by polyhydroxyethylmethacrylate P(HEMAHap) and phytic acid to improve its adsorption capacity for Tb^{3+}. The adsorption kinetics followed the pseudo-second order model and indicated that the rate-controlling step was chemical adsorption. It was observed that the ionic strength did not have any effects on the adsorption capacity of reviewed adsorbents. It was clearly demonstrated that both polyhydroxyethylmethacrylate-modified hydroxyapatite P(HEMAHap) and its modified with phytic acid version P(HEMA–Hap)–phy could be used for separation of Tb^{3+} from aqueous solutions. (Akkaya 2014).

Table 4 – Capacities for Nd, Eu, Tb sorption on novel low-cost adsorbents

Adsorbent	Maximum adsorption capacity, mg/g	Source
Calcium alginate	Nd^{3+} 194.73	Wang et al. 2014
Calcium alginate-poly glutamic acid hybrid gels	Nd^{3+} 238.00	Wang et al. 2014
Magnetic nano-hydroxyapatite	Nd^{3+} 323	Gok 2014
SiO2/UF composite material	Nd^{3+} 8.654 Eu^{3+} 11.652	Naser et al. 2015
Bone powder	Nd^{3+} 10.9 Eu^{3+} 12.7	Butnariu et al. 2015
Chitosan+EDTA	Nd^{3+} 74.4	Roosen & Binnemans 2014
SiO_2	Nd^{3+} 4.808 Eu^{3+} 6.079	Naser et al. 2015
Graphene oxide	Eu^{3+} 142.8	Yao et al. 2016
Sulfonated graphene oxide	Eu^{3+} 125	Yao et al. 2016
Malt spent rootlets	Eu^{3+} 156	Anagnostopoulos et al. 2016
Chitosan nanoparticles	Eu^{3+} 114.9	Cadogan et al. 2014
Raw cactus fibres	Eu^{3+} 0.024	Prodromou & Pashalidis 2016
Modified cactus fibers (phosphorylated)	Eu^{3+} 0.006	Prodromou & Pashalidis 2016
Modified cactus fibres (MnO_2-coated)	Eu^{3+} 0.069	Prodromou & Pashalidis 2016
Activated carbon	Eu^{3+} 86	Anagnostopoulos et al. 2016
Crab shells	Eu^{3+} 3.238	Cadogan et al. 2014
SBA/SA	Eu^{3+} 5.1	Dolyatyari et al. 2015
SBA/EnSA	Eu^{3+} 15.6	Dolyatyari et al. 2015
Fe_3O_4 and cyclodextrin magnetic composite pH = 3.5/5.0	Eu^{3+} 0.007 / 0.012	Guo et al. 2015
EDTA-beta-cyclodextrin	Eu^{3+} 55.62	Zhao et al. 2016
Hydroxyapatite	Eu^{3+} 0.25	Granados-Correa et al. 2013
Thiourea-based hydrogel	Tb^{3+} 64	Reddy et al. 2016
Transcarpathian clinoptilolite	Tb^{3+} 6.1	Vasylechko et al. 2015
Hydroxyapatite	Tb^{3+} 0.038	Akkaya 2014
P(HEMAHap)	Tb^{3+} 0.109	Akkaya 2014
P(HEMA-Hap)-phy	Tb^{3+} 0.049	Akkaya 2014

5. THEORETICAL FRAMEWORK

5.1 Adsorption phenomenon

The phenomenon under review of this thesis is adsorption from the liquid phase. For this case, adsorption involves solid adsorbent, bisphosphonate N10O and aqueous solution, where rare earth metal ions are dissolved. Adsorption occurs when metal ions adhere to the BP, thus virtually removing themselves from liquid phase. This happens after a certain time passes, which is enough for the system adsorbent-adsorbate to establish equilibrium. After the equilibration time, there are no changes in the system, which is supported by equal chemical potential of the adsorbate on the adsorbent surface and in the liquid phase (Sainio 2015). Driving force of adsorption becomes zero as soon as the equilibrium is established.

There are two basic types of sorption: chemical sorption (chemisorption) and physical sorption (physisorption). Very weak (< 50 kJ/mol) interactions indicate van-der-Waals interaction kind and are characteristic of physisorption. This adsorption type forms multiple layers of adsorbate molecules and can be reversed by heating.

Strong interactions (> 50 kJ/mol) indicate ionic, covalent or metallic interactions, depending on the origin (Coulombic or quantum-chemical) and strength level. They form during chemisorption. Typically chemisorption forms monolayer of adsorbate, requires activation energy and cannot be reversed (Tompkins 1978).

Relationship between concentrations of adsorbent and adsorbent is described by adsorption isotherms. General adsorption isotherm form is presented in the equation (1) below: (1)

$$q_e = q_e (C_e, T)$$

Normally, loading of a required species will depend on various factors: temperature, concentration, interactions between adsorbent and adsorbate, interactions in the bulk phase, presence of competing adsorbates (Sainio 2015).

5.2 Adsorption isotherms

Adsorption isotherms provides rapid and concise information about adsorption process. For example, looking at adsorption isotherm one can understand, whether the adsorbent will work in low concentrations of the solute. An estimation about which processes happen can be made. Also the adsorption capacity, which is maximum uptake of the adsorbate, can be noted. According to Giles (1960), there are various types of adsorption isotherms: S (S-type), L (Langmuir), H (high affinity), C (constant partition). They can be seen on the Figure 6.

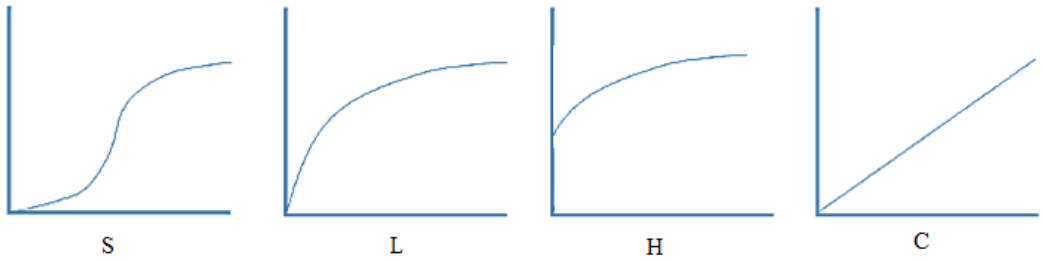

Figure 6 – Types of adsorption isotherms according to Giles, 1960

Giles (1960) further suggested, that type of the isotherm explains the occurring process as follows: C-type shows that affinity of adsorbate to the sorbent is constant, and adsorption sited are not limited. L-type indicates that there is a limit of loading, and as adsorption approaches to full capacity, the process slows down. H-type is a particular case of L-type, where the affinity of solute to the adsorbent is so high that in dilute solution it is totally adsorbed. As for the S-type, three conditions are usually fulfilled: solute molecule is monofunctional and has moderate intermolecular attraction, and there is competition with other molecules for adsorption sites.

When exploring new adsorbent, it is particularly important to understand which adsorption equilibrium correlation is applicable. This will help to predict adsorption parameters and quantitatively compare adsorbents for varied systems or conditions. Adsorption isotherms describe the adsorbate interacts with the adsorbent and are essential for optimizing and designing sorption process. They also give information on such important characteristic as surface properties and the capacity of the adsorbent (Hameed 2008).

In this work, three two-parameter adsorption isotherm models were examined, namely Freundlich, Langmuir, Temkin, as well as three three-parameter isotherms, namely Redlich-Peterson, Toth and Sips isotherms. These models are described below. Equation are cited based on the work of Foo & Hameed (2009). Symbols and coefficients are defined in the List of Symbols and Abbreviations, page 5.

5.2.1 Langmuir isotherm

This model was created by Irving Langmuir in 1916. This model has several assumptions: monolayer coverage only, homogeneous surface of adsorbent, all adsorption sites are equivalent, no interactions between adjacently adsorbed molecules.

This model is the most popular among researchers, because is agrees well with big variety of experimental data (Ho, 2000). As can be seen from the equation (2), at big adsorbate concentrations, the model predicts maximum capacity of adsorption, which is a constant value due to monolayer coverage.

$$q_e = q_m K_L \frac{C_e}{1 + K_L C_e} \tag{2}$$

5.2.2 Freundlich isotherm

It is the earliest known empirical isotherm equation, deduced by Herbert Freundlich in 1906. It can be applied to non-ideal adsorption on heterogeneous surfaces. The model was derived on assumption that adsorption energy decreases logarithmically with filling of adsorption sited. It also allows multiple layers.

The criticism of this model is based on the fact that unlike Langmuir equation it does not reduce to Henry's law at low sorbate concentrations. Therefore, it is better to try fitting experimental data to isotherms with a theoretical basis. Freundlich isotherm can be described by equation (3).

$$q_e = K_F C_e^{\frac{1}{n_f}} \tag{3}$$

5.2.3 Temkin isotherm

This model was empirically created by Mikhail Temkin in 1941. It extends Langmuir model on homogeneous-heterogeneous surfaces. Molecules first adsorb on the sited with higher adsorption heat (energy), therefore adsorption heat decreases linearly with filling of sites. However, this decrease can also happen on homogeneous surface, due to interactions of adsorbed molecules. It can be described by equation (4).

$$q_e = \frac{RT}{b_T}\ln(A_T C_e) \tag{4}$$

5.2.4 Redlich-Peterson isotherm

This isotherm was conceived by Otto Redlich and D.L. Peterson in 1959, and it is a hybrid of Langmuir and Freundlich isotherms. Thus, equation (5) approximates to Henry's law for dilute solutions, and at high concentrations it conforms to Freundlich isotherm (Redlich 1959).

$$q_e = \frac{K_R C_e}{1 + a_r C_e^{b_r}} \tag{5}$$

5.2.5 Toth isotherm

Toth model describes adsorption in heterogeneous systems and comes from theory of potential. The assumption is that energy follows quasi-Gaussian distribution, and there are more high-energy sites than low-energy sites. The model can be described by equation (6):

$$q_e = \frac{K_{Toth} C_e}{(a_{Toth} + C_e)^{\frac{1}{b_{Toth}}}} \tag{6}$$

5.2.6 Sips, or Langmuir-Freundlich isotherm

It was conceived by R. Sips in 1948 for heterogeneous systems and it successfully circumvents problems assocated with Freundlich isotherm in high concentration regions. Sips model, described by equation (7), unites Langmuir and Freundlich in such a way, that at low concentrations it reduces to Freundlich isotherm, and at high concentrations it is able to predict adsorption capacity, as in Langmuir model.

$$q_e = \frac{K_s C_e^{b_s}}{1 + (a_s C_e)^{b_s}} \tag{7}$$

5.3 Modelling adsorption isotherms

Least-squares method has been used by many researchers to fit experimental points to theoretical dataset. This method minimizes sum of squares of errors between experimental and theoretical points. Linear least square method is applied to linear functions, i.e. functions which are linear in parameters. In adsorption modelling, these are isotherms in linearized form. When the function is not linear with respect to unknown parameters, non-linear least squares method is applied, as in the case of non-linearized isotherms.

Previously, linearized isotherms were mostly applied, due to lack of digital data treatment technique and simplicity of linear transformation. However, it has been pointed out that linearization of non-linear functions brings different results based on the method of linearization. This is due to the fact, that linearization changes the error variance of experimental data (Foo & Hameed 2009). For example, Freundlich isotherm can fit the empirical data better at low concentrations, whereas Langmuir exerts better fit at high concentrations. Non-linear regression gives a possibility for more rigorous fit, without violating error variance. However, it is more complex from mathematical point of view. Development of computer technologies allowed to effortlessly fit isotherm parameters without linearization. Consequently, non-linear regression was used in this work.

Optimization procedure defining adsorption isotherm parameters requires an error function (also called objective function, or OF) to minimize. Several error analysis methods have been applied through the years of research on adsorption to define the best-fitting isotherm: squared sum of errors, coefficient of correlation, coefficient of determination, the average relative error, the sum of the absolute errors, chi-squared test, Marquardt's percent standard deviation. However, use of one single error function may be inappropriate (Ho 2004). For example, absolute deviation error function shifts the regression to higher concentration values. Partly this problems can be mitigated by calculating sum of normalized errors.

In order to establish which error function gives the most reliable results, 7 error functions plus sum of normalized errors were calculated for each isotherm model. Then, for each of the three metals apart, the conclusion was made, based on SNE, which of the OF better fits the model to experimental data points. This OF was then used for obtaining isotherm pa-

rameters. The best-fitting isotherm model was again chosen based on SNE. The procedure was described by Raji et al. (2015), and more details are given below.

The trial-and-error procedure was conducted using the solver add-in within Microsoft Excel 2013. Eight error functions were studied and in each case difference between modelled and measured values range was minimized or maximized, as in the cases of determination coefficient and percent of explained variation. Isotherm parameters that were obtained in this way were used to calculate other error functions. These steps were performed for all OF. Afterwards, maximal value for each error function in the row was chosen. Then, values of each function were divided into the maximal value of this function. Normalized results in the region [0;1] for different error functions were obtained. SNE was calculated for each parameter-determining error function. The error functions used are presented in the Table 5.

Table 5 – Error functions, used for fitting adsorption isotherm parameters

Error function	Name	Definition
Coefficient of determination	R2 or R^2	$R2 = \frac{\sum(q_{meas} - \bar{q}_{meas})^2}{\sum(q_{meas} - \bar{q}_{meas})^2 + \sum(q_{meas} - q_{calc})^2}$
Nonlinear chi-square test	χ^2 or Chi2	$\chi^2 = \sum \frac{(q_{meas} - q_{calc})^2}{q_{meas}}$
Residual root mean square error	RMSE	$RMSE = \sqrt{\frac{1}{n_e - 2}\sum(q_{meas} - q_{calc})^2}$
Average relative error	ARE	$ARE = \frac{100}{n_e}\sum\left\lvert\frac{q_{meas} - q_{calc}}{q_{meas}}\right\rvert$
Standard deviation of relative errors	S_{RE}	$S_{RE} = \sqrt{\frac{\sum((q_{meas} - q_{calc}) - ARE)^2}{q_{meas}}}$
Marquardt's percent standard deviation	MPSD	$MPSD = 100\sqrt{\frac{1}{n_e - p}\sum\left(\frac{q_{meas} - q_{calc}}{q_{meas}}\right)^2}$
Sum squares errors	*ERRSQ*	$ERRSQ = \sum(q_{meas} - q_{calc})^2$
Sum of normalized errors	*SNE*	$SNE = \sum_{i=1}^{7}\frac{f_i}{f_i^{max}}$

5.4 Adsorption kinetics

Prior to actually applying the adsorbent, it is indispensable to obtain information about adsorption kinetics. From kinetic data, adsorption rate may be determined. Consequently, residence time of solution in the reaction vessel and size of the adsorption system may be estimated.

Solid-liquid adsorption mechanism explains how the adsorbate proceeds from the initial free state in aqueous solution to adsorbed state on of the sorbent surface.

On its way, the adsorbate passes 4 stages:

1. Transport in bulk solution
2. Diffusion through the liquid film around adsorbent particles (external diffusion)
3. Diffusion through the pores of the adsorbent particles (intra-particle diffusion)
4. Chemical reaction of adsorption on the surface of the adsorbent (mass action)

This mechanism is schematically represented by the Figure 6.

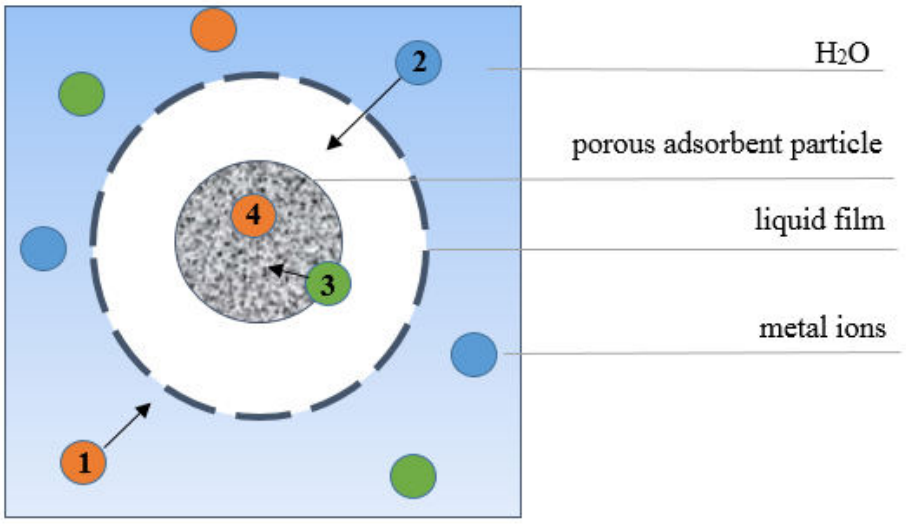

Figure 6 – Steps of adsorption process (Kumar 2014)

For physical sorption, mass action is very fast and thus can be neglected. However, for models that come from chemical reaction kinetics, the whole process of adsorption is taken into account, and these four steps are not distinguished.

Given the information above, all the models describing adsorption kinetics can be divided into 2 groups: diffusion models and reaction models. Diffusion models include Liquid Film Diffusion, Intra-particle Diffusion and Double Exponential equations. Reaction models comprise Pseudo-first-order, Pseudo-second-order, Elovich and Second-order equations.

If the slowest step of the whole process is chemical sorption, the reaction occurs between the adsorbate particle and the free site. The adsorption progress is shown in the Table 6 (Largitte & Pasquier 2016).

Table 6 – Adsorption progress

	Adsorbate +	Free site	$\underset{k_{-1}}{\overset{k_1'}{\rightleftarrows}}$	Occupied site
t=0	C_0	q_{max}		0
t	C_t	q_{max}-q_t		q_t
t_{eq}	C_{eq}	q_{max}-q_{eq}		q_{eq}

According to the progress of adsorption, the differential equation (8) can be written:

$$\frac{d(q)}{dt} = k_1'(C_t)^m(q_{max} - q)^n - k_{-1}(q)^n \tag{8}$$

If Ct is constant, the equation simplifies into (9):

$$\frac{d(q)}{dt} = k_{r1}(q_{max} - q)^n - k_{r-1}(q)^n \tag{9}$$

If the reaction order is 1 and there is no desorption, equation (9) yields Lagergren equation (Pseudo-first-order equation). With order equaling 2, it becomes Pseudo-second-order equation. In this work, pseudo-first-order equation, pseudo-first-order equation and Elovich equation are used.

Diffusion models assume that rate-determining step of adsorption process is either liquid film diffusion or intra-particle diffusion (Qiu 2009). For assessing probability of liquid film diffusion as controlling stage, Linear Driving Force Rate or Film Diffusion Mass Transfer equation (Boyd equation) are used. For intra-particle diffusion, the equations ap-

plied are Homogeneous Solid Diffusion Model, Dumwald-Wagner and Weber-Morris. When adsorption mechanism involves both film diffusion and intra-particle diffusion, Double-exponential model is used. Review of recent literature about showed that the equations which successfully describe adsorption of heavy metals are Boyd and Weber-Morris equations (Okewale 2013 etc.).

Overall rate of adsorption by diffusion coupled with reaction depends on diffusivity. Diffusivity can be estimated via Shrinking Core Model. This model establishes equations for different rate determining steps. It would be applicable for the scope of this thesis if only the particles of the adsorbent would have been spherical. Other assumptions of the shrinking core model, i.e. similar particle size and constant concentration on the adsorbent surface are kept. The dimensions of N10O particles are 5x30x50 μm, which makes obvious that the microcrystals of the BP resemble tiny needles and thus cannot be considered spherical.

5.4.1 Pseudo-first-order equation

In 1898 Lagergren presented the earliest first-order rate model describing liquid-solid adsorption. It can be presented as follows:

$$\frac{dq_t}{dt} = k_1(q_e - q_t) \tag{10}$$

Integrating and rearranging the equation (10) leads to equation (11), as shown by Ho (2004):

$$\log(q_e - q_t) = logq_e - \frac{k_1}{2.303}t \tag{11}$$

If equation (11) is valid, the plot $\log(q_e\text{-}q_t)$ versus t should represent a straight line. Alternatively, non-linear regression may be applied to another form of pseudo-first-order model, shown in the equation (12):

$$q = q_e(1 - e^{-k_1 t}) \tag{12}$$

5.4.2 Pseudo-second-order equation

Pseudo-second-rate equation was described by Ho (1995). If the adsorption system follows a pseudo-second order kinetics, which means two sites per adsorbate, rate determining step may be chemisorption involving valent forces, sharing or exchange of electrons between the sorbent and adsorbate. Moreover, the adsorption should follow Langmuir equation. The rate equation is presented below:

$$\frac{dq_t}{dt} = k_2(q_e - q_t)^2 \tag{13}$$

Rearrangement of (13) gives equation (14):

$$\frac{t}{q_t} = \frac{1}{V_0} + \frac{1}{q_e}t \tag{14}$$

Where: V_0 – initial adsorption rate, mg/(g·min), given by (15):

$$V_0 = k_2 q_e^2 \tag{15}$$

The constants can be found via plotting t/q_t versus t. If the Pseudo-second-order applies, the plot should give straight line. Alternatively, non-linear regression may be applied to another form of pseudo-second-order model, shown in the equation (16):

$$q = \frac{q_e^2 k_2 t}{1 + q_e k_2 t} \tag{16}$$

To underline the difference between capacity- and concentration-based models, the Lagergren equation and equation (13) are called pseudo-first-order and pseudo-second order equations correspondingly.

5.4.3 Elovich equation

Elovich equation was created by Zeldowitch and Roginskii in 1934. It describes chemisorption with activation on heterogeneous surface. Initially it was applied for gas adsorption onto solid sorbents. However, in a number of publications Elovich equation was found appropriate for describing heavy metal uptake from aqueous solutions (Fierro et al. 2008). The equation of Elovich model is presented below (Ho 1998):

$$\frac{dq}{dt} = \alpha e^{-aq} \tag{17}$$

Elovich equation can be rearranged to obtain equation (18):

$$q_t = \alpha \ln(a\alpha) + \alpha lnt \tag{18}$$

The plot q_t versus lnt should yield straight line if Elovich equation applies.

5.4.4 Film diffusion mass transfer rate equation (Boyd equation)

The equation of liquid film mass transfer was created by Boyd in 1947, and can be presented as follows:

$$\frac{q_t}{q_e} = 1 - \frac{6}{\pi^2}\exp(-B_t) \tag{19}$$

It can also be rearranged:

$$B_t = -0.4977 - \ln(1 - \frac{q_t}{q_e}) \tag{20}$$

Linearity of the plot of Bt versus times shows that film diffusion controls the adsorption process. In the case on intra-particle diffusion the plot passes through the origin.

5.4.5 Intra-particle diffusion model (Weber-Morris equation)

Intra-particle diffusion model is presented by Weber-Morris equations as follows:

$$q_t = k_{diff} t^{\frac{1}{2}} \tag{21}$$

The plot of q_t versus $t^{1/2}$ should represent straight line if intra-particle diffusion is the sole rate-determining step. Otherwise, adsorption kinetics is controlled simultaneously by film diffusion and intra-particle diffusion.

5.5 Selectivity of adsorption

For adsorption process, it is necessary to know how selective the separation is. Separation coefficients were calculated using formulas below. Distribution ratio is calculated by (22):

$$D = \frac{C}{C_s} \tag{22}$$

Then, the selectivity coefficient is calculated by (23):

$$\alpha_{A/B} = \frac{D_A}{D_B} \tag{23}$$

6. EXPERIMENTAL

6.1 General methods

Synthetic solutions of REM were prepared using rare earth metal oxides Nd (III) oxide, Eu (III) oxide, Tb (III, IV) oxide produced by Sigma-Aldrich, with purity 99.9 % trace metal basis. The BP was provided by the research group of Jouko Vepsäläinen from University of Eastern Finland. Acid solutions were prepared using Titrisol or Normadose concentrates. Concentration of acid and base solutions was verified by automatic titrator Mettler Toledo T50.

All the components were weighed using balances Scaltec SBC 31 or Radwag AS 220/X. Density of liquid components was measured by density meter Anton Paar DMA 4500. Volume of liquid components was calculated based on density and mass measurements in order to eliminate possible pipetting error. The concentrated solutions were made up by weight and the less concentrated were prepared by dilution. Solid salt reagents were provided by Sigma Aldrich and distilled water came from laboratory installation. Samples were stirred in Heidolph Promax 2020 shaker.

For pH measurement, pH-meter Consort C3010 was used. The pH-meter was calibrated on solutions known ionic strength. The results are reported as adsorption efficiency dependent on negative logarithm of acid molarity. REM oxides were dissolved together or separately in acid solutions to create a multimetal or single-metal solution of known concentration. For better dissolution, volumetric flask containing REM powder and acid was stirred with magnetic stirrer and heated up to 50 °C for several hours.

The pH was adjusted with 1M NaOH or with acid of appropriate concentration corresponding to matrix solution. Ionic strength of the solution was adjusted by adding NaCl of a needed concentration.

The recovery percent of metal ions in samples was calculated from initial and final metal ion concentrations. Metal ion concentrations in samples were analyzed by Agilent 7900 ICP-MS system in full-quantitative mode. Comparison samples were prepared in the same

manner but without addition of BP, in order to know initial concentrations. Prior to analysis, solids-containing samples were filtered by syringe filter Phenex RC 0.45 µm.

Unless stated otherwise, the samples were fully equilibrated by shaking, then centrifuged, diluted and analyzed by ICP-MS, all in room temperature and normal pressure.

Extraction percent, i.e. percent of extracted metals, was calculated by equation (24).

$$E\% = \frac{c_{initial} - c_{final}}{c_{initial}} \cdot 100 \tag{24}$$

Loading was calculated by equation (25):

$$q = \frac{(C_0 - C_{e)} \cdot V_{sample}}{m_{adsorbent}} \tag{25}$$

Ionic strength was calculated by equation below:

$$I = \frac{1}{2}\sum_{i=1}^{n} c_i z_i^2 \tag{26}$$

6.2 pH isotherms

Efficiency of recovery REM from multimetal aqueous solutions was studied as a function of pH (or hydrogen ion concentration). Experiment was conducted in 12 ml glass test tubes, in atmospheric pressure and room temperature. Rare earth metal oxides were dissolved in 1M HCl, 1M HNO_3, and 0.5 M H_2SO_4 in order to achieve 500 ppm of each REM.

To each test tube, REM stock solution, NaCl, H_2O and NaOH were added in order to obtain series of samples with the ionic strength equaling 1 and similar REM concentration but different pH. Then 0.2 g of the adsorbent N10O was added to each sample. After that, test tubes were agitated for 24 hours. Samples were centrifuged by laboratory centrifuge Heraeus Megafuge 1.0, then filtered by syringe filter Phenex RC 0.45 µm and analyzed by ICP-MS.

The pH-meter was calibrated on solutions with ionic strength 1 and varying pH. There were 6 calibration solutions, prepared by adding together known amounts of acid, water and salt. Calibration curve for HCl matrix can be seen on the Figure 7.

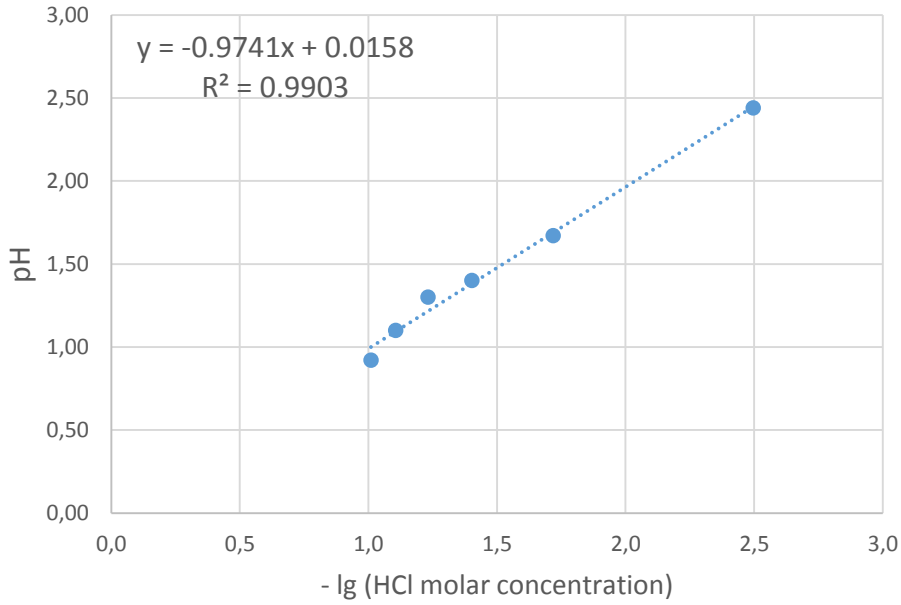

Figure 7 – Calibration curve for dependence of pH on HCl molar concentration

6.3 Adsorption kinetics

To understand the kinetics of adsorption process, series of samples with similar concentrations and excess of adsorbent were prepared. Stock multimetal solution with concentration of Nd, Eu, Tb equal to 40 ppm was made in a 200 ml beaker. Then the pH was adjusted to 1.5, and excess of BP was added to the reactor. Prepared in such a manner, similar samples were stirred in a shaker, after certain time one sample was taken out and filtered. Afterwards, ICP-MS analysis was conducted.

6.4 Temperature dependence of adsorption

Experiment was conducted in 12 ml test tubes, in atmospheric pressure with the optimal pH= 1.3. Oxides of REM oxide were separately dissolved in 1M hydrochloric acid to create a multimetal solution of 500 ppm of each Me. Ionic strength of the solution was kept constant by adding NaCl of appropriate concentration. After adding 0.2 g of N10O adsor-

bent, samples were agitated for 24 hours for preliminary equilibration. Then samples were gradually heated to certain temperature at constant stirring.

6.5 Loading isotherms

To visualize adsorption isotherms, the experiment was conducted in test tubes, in atmospheric pressure and room temperature, with excess of N10O. First approach was to have different amount of adsorbent in each test-tube, while keeping initial concentration of metal in the solution constant. However, in this manner no general trend was observed. This may be explained by the fact, that for such small scale, significant amount of adsorbent was dissolved. Therefore, different approach was applied: keeping BP amount constant but varying metal concentrations in test tubes.

To each 12 ml glass test tube, 2000-5000 ppm single-metal solution in 1M HCl matrix was added. By diluting with H_2O, series of samples with different rare earth metal content was prepared. Ionic strength was constant, as well as pH=2. In total, 47 samples were made for each REM. After adding 0.2 g of the adsorbent N10O, samples with varying concentrations of metal ions were agitated for 24 hours.

6.6 Ionic strength

To establish adsorption dependence on ionic strength, three series of data points were created. The series had 6 samples each and ionic strength values of 0.5 M, 1.88 M and 3.22 M. In each sample, the pH varied from 0.5 to 8. Ionic strength was adjusted by adding NaCl. Oxides of REM oxides were separately dissolved in 1M hydrochloric acid to create a multimetal solution of 200 ppm of each REM. After adding 0.2 g of adsorbent, samples were agitated for 24 hours for full equilibration. Experiment was conducted in 12 ml glass test tubes, in atmospheric pressure and room temperature.

7. RESULTS AND DISCUSSION

7.1 pH isotherms

In total, 48 samples in HCl, 11 samples in HNO_3 and 11 samples in H_2SO_4 were made, covering pH range from 0.8 to 12.5 for HCl and from 0.5 to 3.5 for HNO_3 and H_2SO_4. Results of pH dependence experiments in HCl, HNO_3 and H_2SO_4 are shown on the Figures 8-10. The plots are presented as adsorption efficiency dependent on negative logarithm of acid molarity.

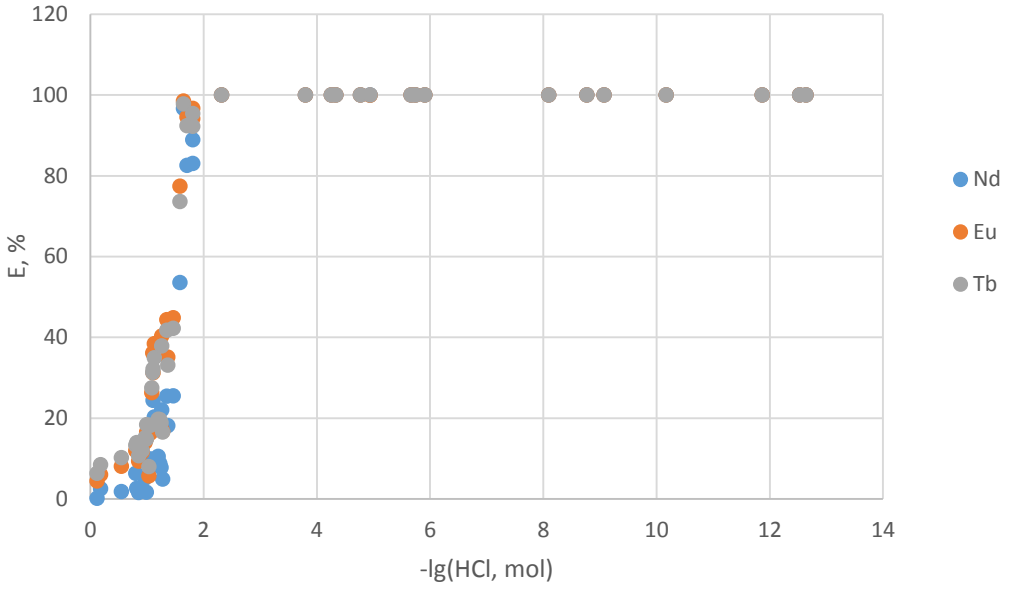

Figure 8 – pH isotherm for Nd, Eu, Tb adsorption on N10O from 1M HCl.[1]

1 - For experimental conditions, refer to the Section 6.2

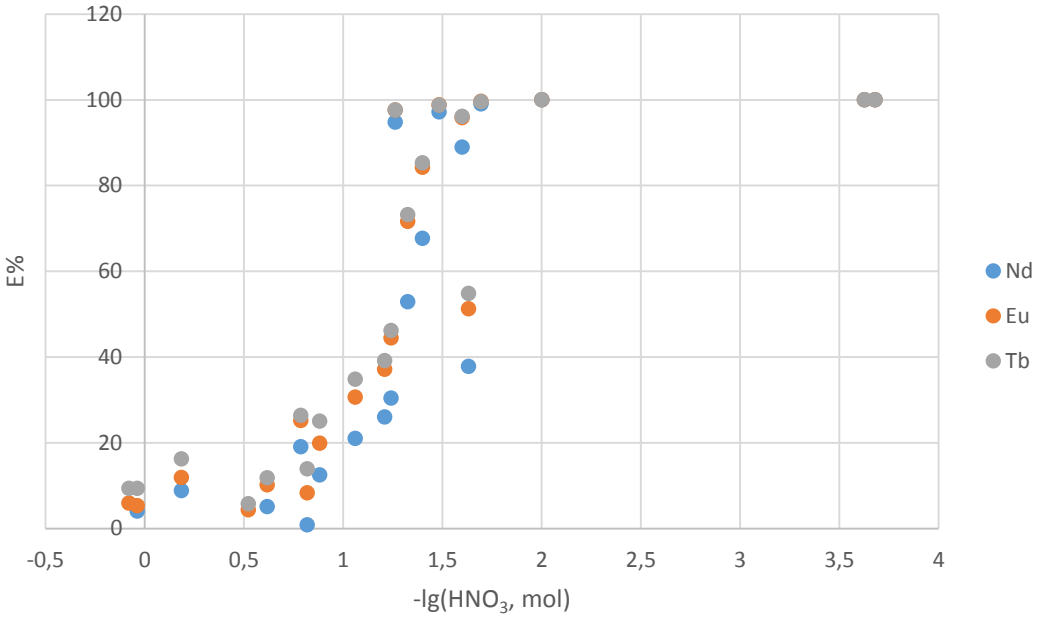

Figure 9 – pH isotherm for Nd, Eu, Tb adsorption on N10O from 1M HNO_3[1]

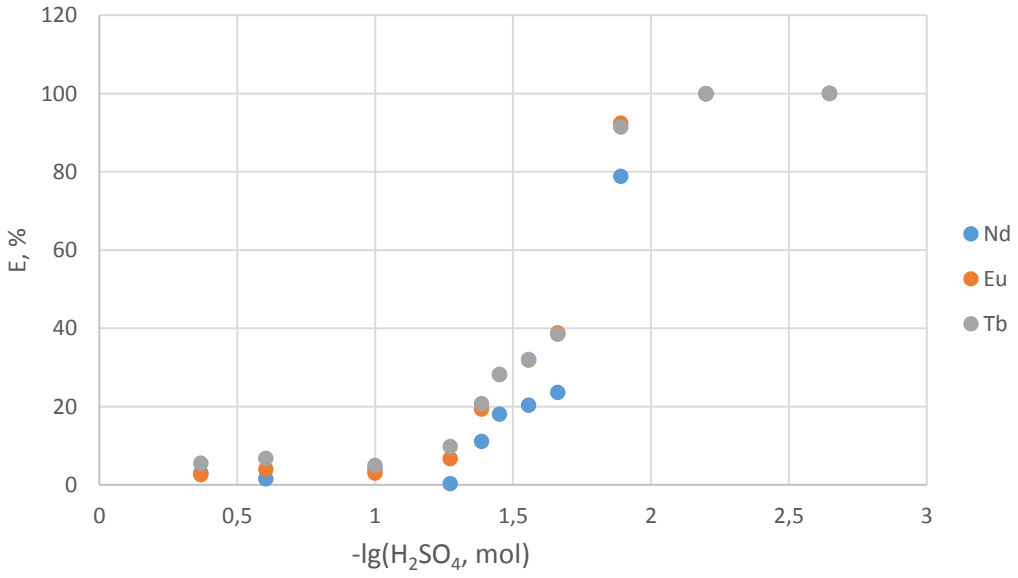

Figure 10 – pH isotherm for Nd, Eu, Tb adsorption on N10O from 0.5 M H_2SO_4[1]

1 - For experimental conditions, refer to the Section 6.2

7.2 Adsorption kinetics

Experiment results are shown on the Figure 11 and Figure 12 as adsorbent loading depending on time and extraction percentage depending on time.

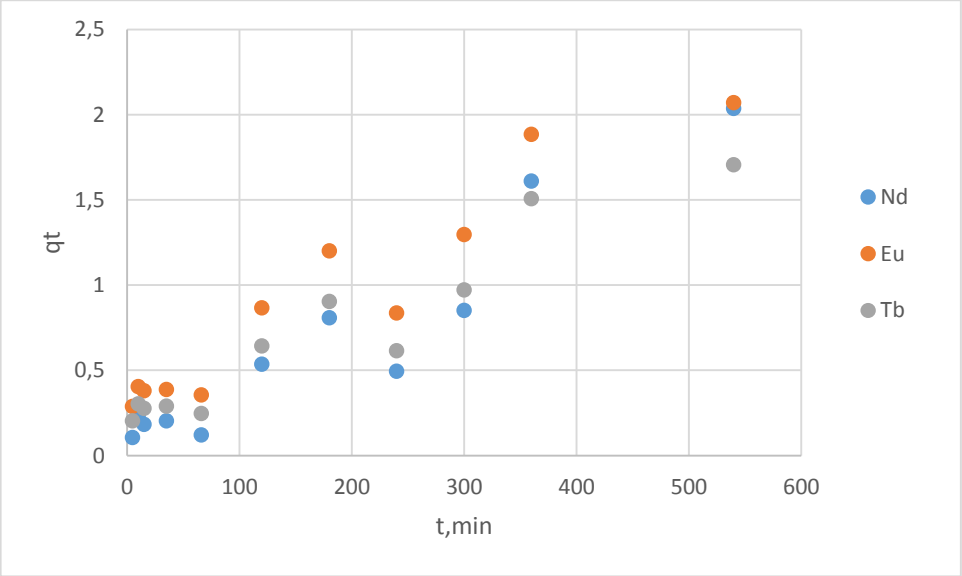

Figure 11 – Adsorption loading dependence on time for Nd, Eu, Tb adsorption on N10O from 1M HCl, pH=1.5[1]

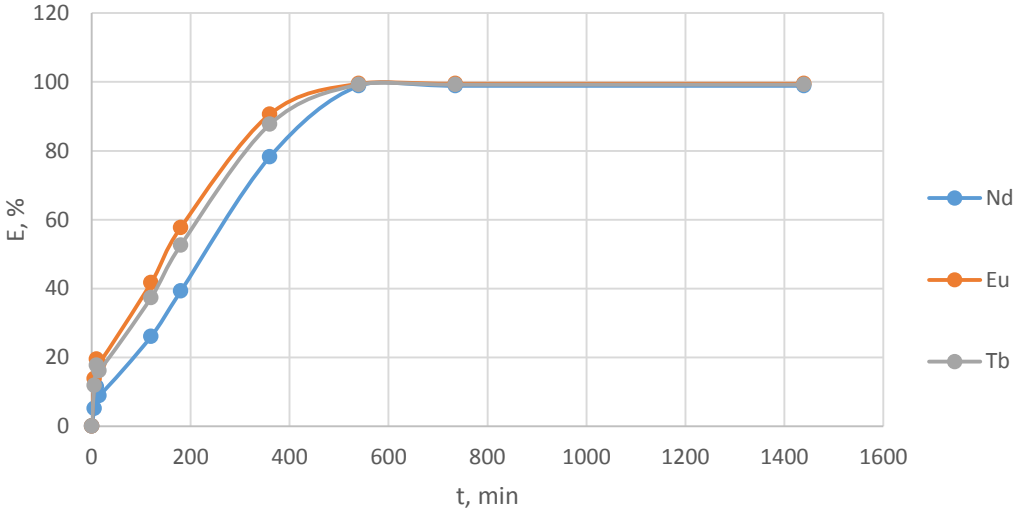

Figure 12 – Extraction percent dependence on time for Nd, Eu, Tb adsorption on N10O from 1M HCl, pH=1.5[1]

As shown on the Figure 12, adsorption rate was high in first 9 hours. Afterwards, when at 540th minute 98% or metals were adsorbed, the rate decreased to nearly constant value. This might be explained by the fact that in the beginning, plenty of empty sited are ready to

1 - For experimental conditions, refer to the Section 6.3

adsorb metal ions. Also, the pH decrease was noticeable, even after short 30 min equilibration. This is due to the fact that hydrogen ion in the side chain of the bisphosphonate displaced metal ion by ion exchange. As hydrogen ions are released into solution, the pH decreases. As the process goes on, there are less sites, so the adsorption slows down.

7.2.1 Reaction models

Although both linearized and non-linear versions of reaction model equations were used for fitting the experimental data, it was clear that the use of non-linear regression was more reliable. This was also confirmed by research papers (Lin & Wang 2009).

Non-linear regression was performed via maximizing determination coefficient for Pseudo-first-order equation, Pseudo-second-order equation and Elovich equation. Resulting plots are presented in the Figure 13[1]. Coefficients of determination and rate constants can be found in the Table 7.

a)

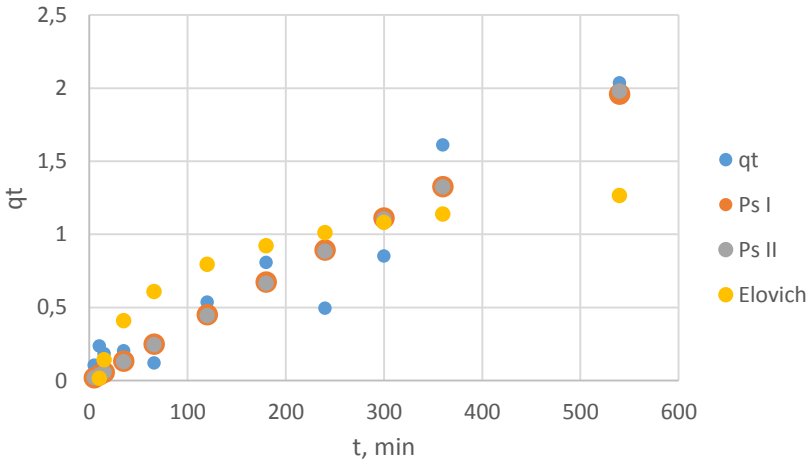

b)

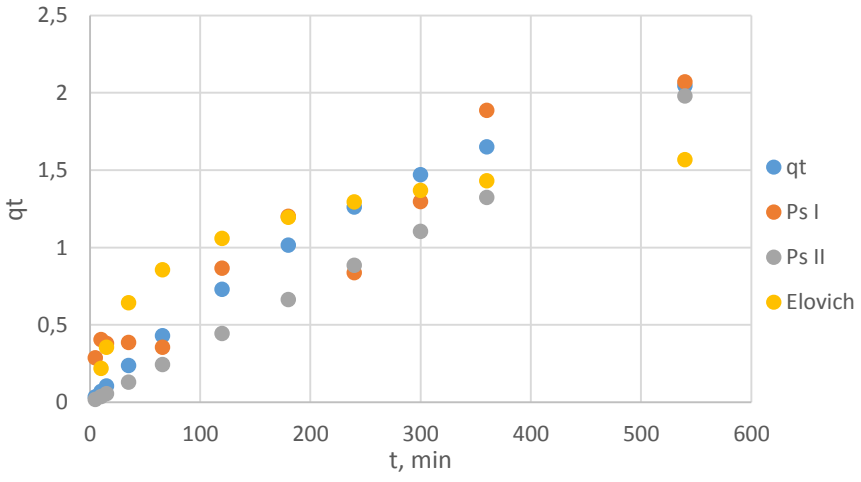

1 - For experimental conditions, refer to the Section 6.3

c)

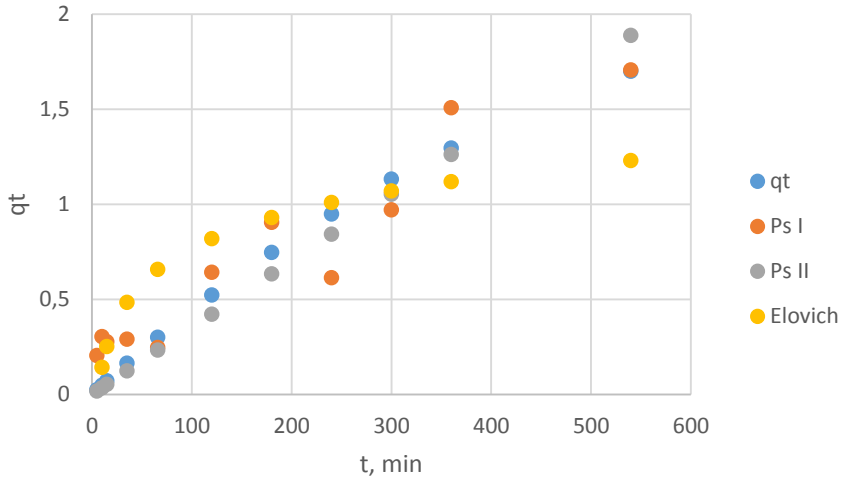

Figure 13 – Experimental loading and loading from pseudo-first-order, pseudo-second-order mode and Elovich model for a) Nd b) Eu c) Tb adsorption on N10O[1]

It can be seen from the table 1 that q_e, i.e. equilibrium loading is several orders of magnitude lower than those obtained by loading experiments. This issue was assumed by Plazinsky (2013): correct values of adsorbent capacity are obtained only when experimental points are close to q_e, whereas for low solute concentrations kinetic models predict local maximum of adsorption capacity: adsorption capacity in given condition. However, it is important to present the kinetic data also for lower concentrations, otherwise the overall data interpretation can fail (Haerifar 2013). It can be noted from the Table 8, that the correlation coefficients for pseudo-first-order model are slightly higher than those for the other two models. This can be explained by the fact that surface coverage of the adsorbent is relatively scarcely covered, compared to its full capacity. The applicability of pseudo-first-order model for initial times of adsorption and for the cases where equilibrium coverage is small was shown by Haerifar (2013) and Marzcevski (2010).

On the other hand, the results to not comply with those provided by University of Eastern Finland (Alanne 2014). Excessively small driving force might be attributed to the experimental conditions, which do not disclose real speed of adsorption.

7.2.2 Diffusion models

In order to predict the rate determining the diffusion mechanism, intra-particle diffusion model and Boyd models were used. The plot of q_t versus $t^{1/2}$ for Weber-Morris model was constructed, and it was linear with high reliability (R^2=0.8) but did not pass through the

1 - For experimental conditions, refer to the Section 6.3

origin for any metals as shown on the Figure 14. The intercept was slightly negative. It means that some other mechanism apart from intra-particle diffusion is involved into sorption, such as film diffusion.

The plot of B_t versus time for Boyd model on the Figure 15 was found linear (R^2=0,90), but it neither passed through the origin. Therefore, it can be concluded that rate-controlling process is particle diffusion (Kumar 2014). Liquid film diffusion combines with particle diffusion in case of ion exchange process (Albadarin 2011). Coefficients of determination and model constants can be found in the Table 7.

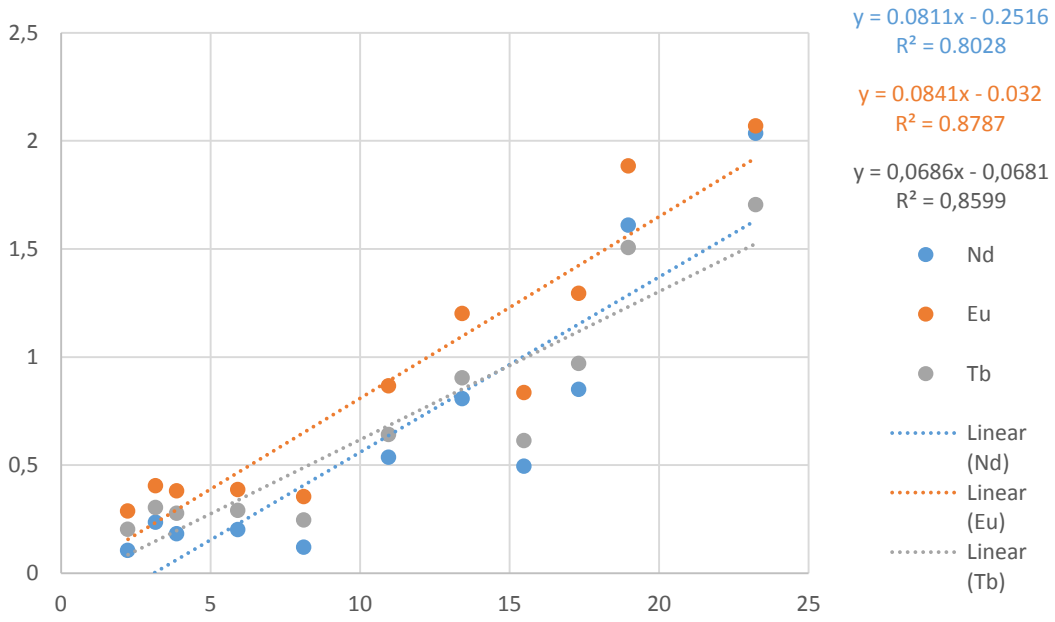

Figure 14 – Intra-particle diffusion model (Weber-Morris model) for Nd, Eu, Tb adsorption from aqueous solutions on the N10O[1]

1 - For experimental conditions, refer to the Section 6.3

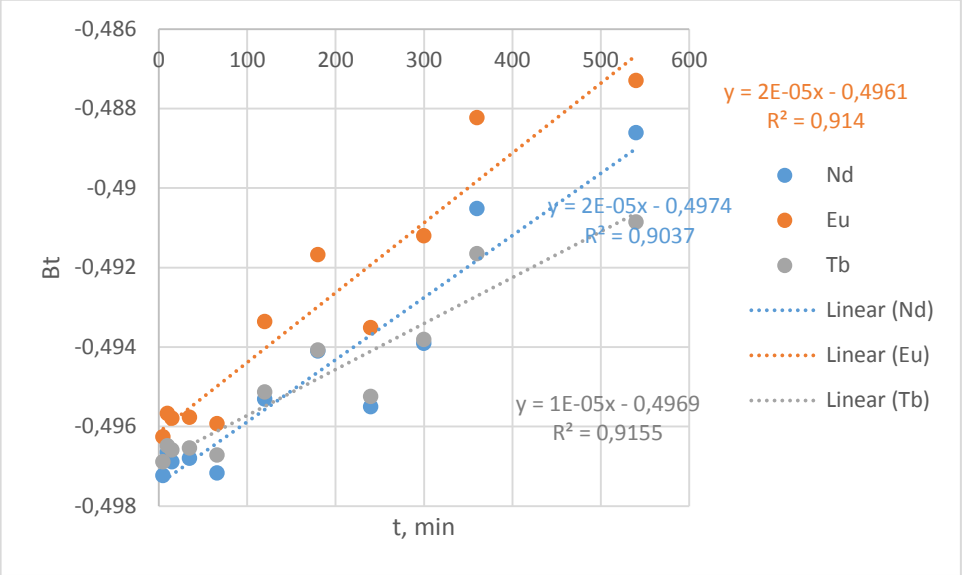

Figure 15 – Film diffusion mass transfer model (Boyd model) for Nd, Eu, Tb adsorption from aqueous solutions on the N10O[1]

1 - For experimental conditions, refer to the Section 6.3

Table 7 – Constants and R^2 for diffusion and reaction kinetic models of Nd, Eu, Tb adsorption on N10O[1]

Me	Pseudo-first-order	Pseudo-second-order	Elovich	Boyd	Weber-Morris
Nd	q_e = 3.94 mg/g k_1=0.0013 min^{-1} R^2=0.98	q_e = 6.92 mg/g k_2=0.00011 g/(mg·min) V_0=0.09 mg/(g·min) R^2=0.97	a=0.33 g/mg α=0.31 mg/(g·min) R^2=0.71	B=0.00002 R^2 = 0.90	k_{diff} = 0.08 C = -0.25 R^2 = 0.80
Eu	q_e = 2.7 mg/g k_1=0.002 min^{-1} R^2=0.87	q_e = 3.94 mg/g k_2=0.0004 g/(mg·min) V_0=0.02 mg/(g·min) R^2=0.86	a=0.56 g/mg α=0.33 mg/(g·min) R^2=0.77	B=0.00002 R^2 = 0.91	k_{diff} = 0.08 C = -0.03 R^2 = 0.88
Tb	q_e = 2.8 mg/g k_1=0.0017 min^{-1} R^2=0.87	q_e = 4.5 mg/g k_2=0.00024 g/(mg·min) V_0=0.01 mg/(g·min) R^2=0.86	a=0.61 g/mg α=0.27 mg/(g·min) R^2=0.78	B=0.00001 R^2 = 0.91	k_{diff} = 0.08 C = -0.85 R^2 = 0.86

7.3 Temperature dependence of adsorption

Resulting plot is shown on the Figure 14.

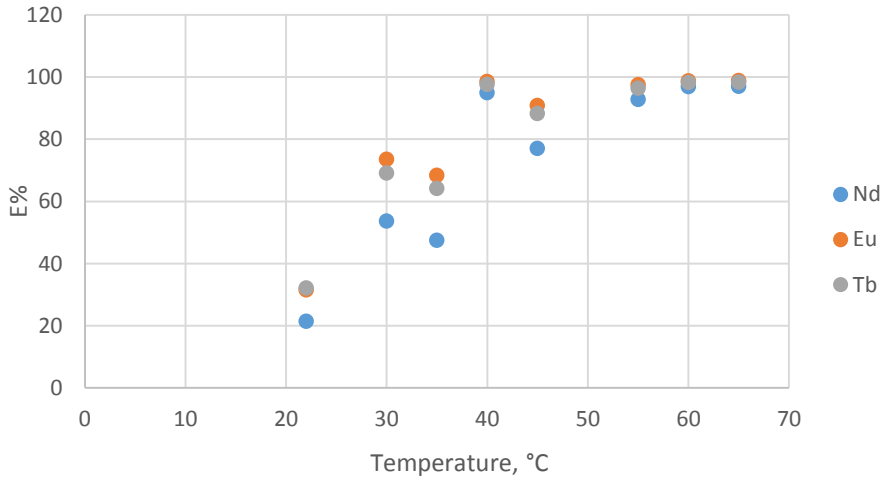

Figure 14 – Extraction percent of Nd, Eu, Tb as function of temperature[2]

1 - For experimental conditions, refer to the Section 6.3
2 - For experimental conditions, refer to the Section 6.4

It can be seen from the plot on the Figure 14, that adsorption is enhanced by temperature. There is some scattering of data points, but it is clear that first temperature where 100% extraction is achieved is 40 °C. This indicated that the type of sorption is chemical sorption.

7.4 Adsorption isotherms

Loading experiments turned out complicated to perform. First, the quantity of the adsorbent was changed. But as the batch mode was chosen, small quantities of the BP had to be added. Therefore, nearly all the bisphosphonate was dissolved. Afterwards, it was also challenging to obtain points in the needed range due to the pH drift, caused by acidity of bisphosphonates. After several experiments, the following loading isotherms were obtained (Figure 15).

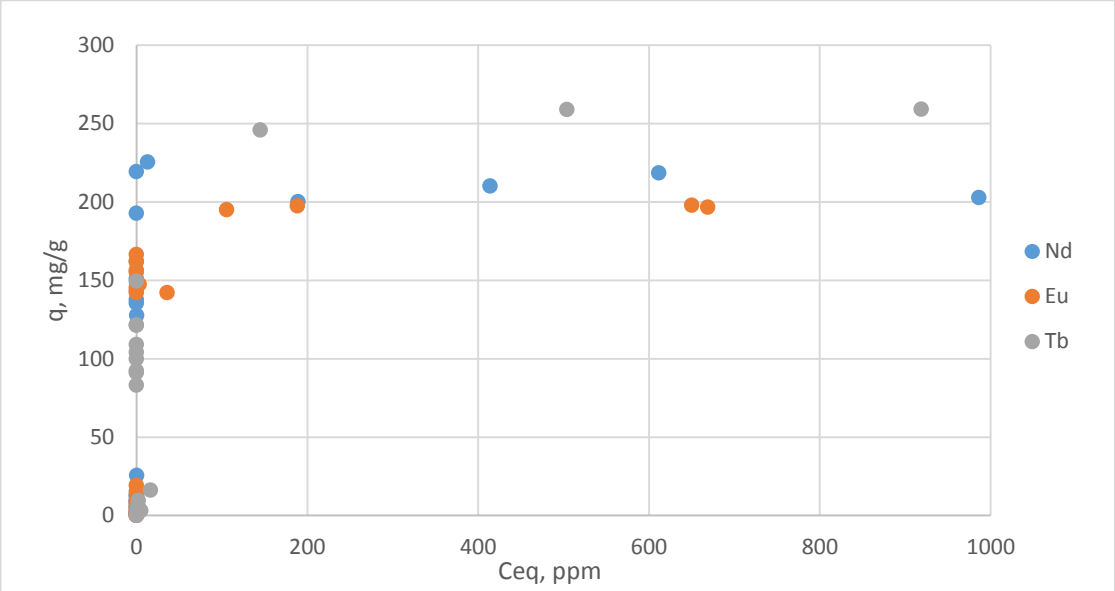

Figure 15 – Loading isotherms for adsorption of Nd, Eu, Tb from aqueous solution by N10O[1]

7.5 Modelling of adsorption isotherms

Most widely used adsorption isotherms models were used to fit the experimental data from the loading experiments. Methods of fitting and theoretical assumptions of adsorption isotherms are explained in the Section 5.

1 - For experimental conditions, refer to the Section 6.5

7.5.1 Neodymium

After having obtained experimental results, three two-parameter and three three-parameter adsorption models were used to fit the data. The best-fitting isotherms were chosen based on appropriate objective function (Explained in detail in Section 5). Seven objective functions were tested for each adsorption model. SNE function was used to establish which objective function gives the best fit. For Neodymium, it was clear from SNE values, that Chi2 gives the best fit for all the models except for Temkin. The plot of loading versus concentration of Nd(III) in the liquid phase for five isotherm models is presented on the Figure 16.

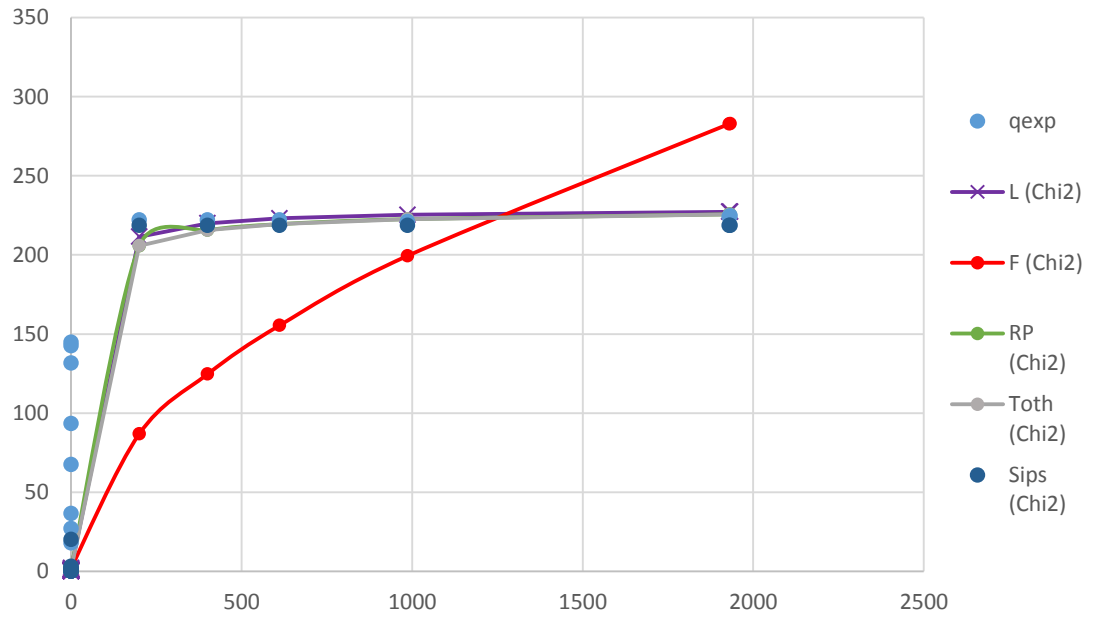

Figure 16 – Adsorption isotherms for Nd(III) uptake by the adsorbent N10O, fitted via Chi2 error function[1]

Langmuir isotherm was fitted to experimental data. Based on SNE, the best fit is provided by Chi2 error function. However, the highest determination coefficient is obtained from R2 and RMSE functions, which is due to big amount of points near the origin. Langmuir isotherm fits the data rather well, with R2=0.70.

1 - For experimental conditions, refer to the Section 6.5

Freundlich isotherm model was fitted to experimental data. Results for error values can be seen in the Table B2. Obviously, Freundlich cannot fit given adsorption process. This is also the case for Temkin isotherm.

The plots of Redlich-Peterson isotherm, Toth isotherm and Sips isotherm show quite good fit, which can be explained by the fact that now there are 3 parameters. Determination coefficients are similar to Langmuir isotherm: 0.69 – 0.70. However, the lowest value for SNE is achieved for Sips isotherm, together with the best R2.

In order to understand which isotherm better fits the experimental data, normalized errors were calculated for each model. The results can be found in the Table 8. It is obvious from SNE values that Sips isotherm gives the best fit. However, Toth and Redlich-Peterson isotherm follow closely. Also there is big difference in the error functions for three- and two-parameter isotherm.

Table 8 - Errors and normalized errors for adsorption isotherms under review for Nd adsorption. Fitting of experimental data is made by Chi2 objective function[1]

	L	F	T	RP	Toth	Sips
	Chi2	Chi2	Chi2	Chi2	Chi2	Chi2
R2	0.70	0.61	0.32	0.69	0.69	0.70
chi2	652.93	829.38	1973.02	652.60	652.60	631.81
RMSE	62.19	77.11	227.50	63.90	63.90	63.64
ARE	101.54	268.54	182.01	98.34	98.22	89.10
Sre	85.77	241.04	195.60	85.40	85.30	79.12
MPSD	158.64	436.92	147.05	151.96	151.75	167.11
ERRSQ	73490	107032	362290.70	73496.70	73498.65	72893.98
normalized errors						
R2	1.000	0.871	0.451	0.992	0.992	0.994
chi2	0.331	0.420	1.000	0.331	0.331	0.320
RMSE	0.273	0.339	1.000	0.281	0.281	0.280
ARE	0.378	1.000	0.678	0.366	0.366	0.332
Sre	0.356	1.000	0.812	0.354	0.354	0.328
MPSD	0.363	1.000	0.337	0.348	0.347	0.382
ERRSQ	0.203	0.295	1.000	0.203	0.203	0.201
SNE	2.904	4.925	5.277	2.875	2.873	2.838

1 - For experimental conditions, refer to the Section 6.5

7.5.2 Europium

After having obtained experimental results, 6 adsorption models were used to fit the data. The best-fitting isotherms were chosen based on appropriate objective functions. For Europium, as well as for Neodymium, it was clear from SNE values, that Chi2 gives the best fit for all the models. The plot of loading versus concentration of Eu(III) in the liquid phase for all isotherm models is presented on the Figure 17.

Langmuir isotherm plot shows that Langmuir model can describe adsorption behavior for Eu. Experimental data is described quite well, with determination coefficient equaling 0.95.

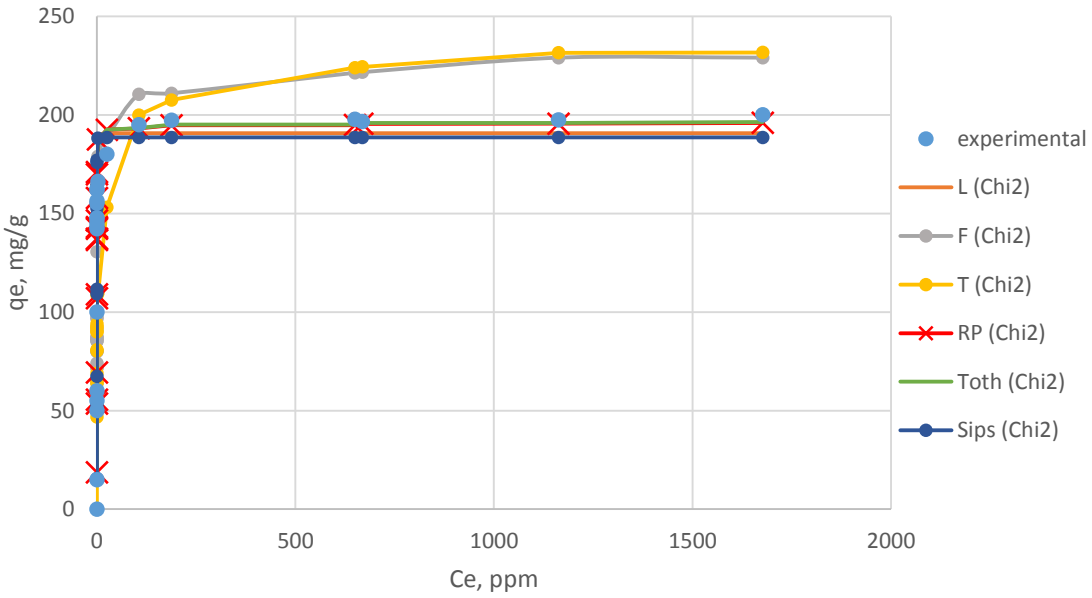

Figure 17 – Adsorption isotherms for Eu(III) uptake by the adsorbent N10O, fitted via Chi2 error function[1]

Determination coefficient for Freundlich and Temkin isotherms equal 0.60 and 0.64 correspondingly. Examination of the plot proves that among 2-parameter isotherms, Langmuir gives the best fit, and Freundlich and Temkin cannot be used for data modelling.

Three-parameter isotherms allow to fit the data well. Such a good fit can be explained by introduction of the third parameter. Determination coefficients are high, and SNE values

1 - For experimental conditions, refer to the Section 6.5

are low. Among two-parameter isotherms, just the Langmuir isotherm can be compared with three-parameter isotherms. The very best fit is provided by Sips isotherm.

The assessment of goodness-of-fit of the isotherms for Eu adsorption is presented in the Table 9. From the SNE values it can be In case of Eu(III), experimental points were more consistent than for Nd(III), therefore overall fit is better than for Neodymium, average R2 being 0,88 as opposed to 0,68 for Nd(III).

Table 9 - Errors and normalized errors for adsorption isotherms under review for Eu adsorption. Fitting of experimental data is made by Chi2 objective function.[1]

	Langmuir	Freundlich	Temkin	Redlich-Peterson	Toth	Sips
	Chi2	Chi2	Chi2	Chi2	Chi2	Chi2
R2	0.95	0.60	0.64	0.95	0.95	0.95
Chi2	23.85	439.56	299.27	22.33	22.13	22.91
RMSE	12.93	45.78	41.80	12.14	12.07	12.90
ARE	6.31	39.19	31.30	6.26	6.23	5.91
Sre	13.63	44.39	42.38	12.93	12.86	13.47
MPSD	9.76	77.53	53.73	10.52	10.49	8.97
ERRSQ	3509.36	44020.59	36689.91	3096.94	3061.42	3494
normalized errors						
R2	0.99	0.62	0.67	1.00	1.00	0.99
Chi2	0.05	1.00	0.68	0.05	0.05	0.05
RMSE	0.28	1.00	0.91	0.27	0.26	0.28
ARE	0.16	1.00	0.80	0.16	0.16	0.15
Sre	0.31	1.00	0.95	0.29	0.29	0.30
MPSD	0.13	1.00	0.69	0.14	0.14	0.12
ERRSQ	0.08	1.00	0.83	0.07	0.07	0.08
SNE	2.00	6.62	5.54	1.97	1.97	1.98

7.5.3 Terbium

The best-fitting isotherms were chosen based on appropriate objective functions. For Terbium, as well as for Europium and Neodymium, it was clear from SNE values, that Chi2 gives the best fit for all the models. The plot of loading versus concentration of Tb(III) in the liquid phase for all isotherm models is presented on the Figure 18.

1 - For experimental conditions, refer to the Section 6.5

Although the experimental data points are scarce, the overall R2 varies from 0.82 to 0.91, which is quite good. Best fit is provided by Sips isotherm, second-best and third-best being Redlich-Peterson and Langmuir isotherms.

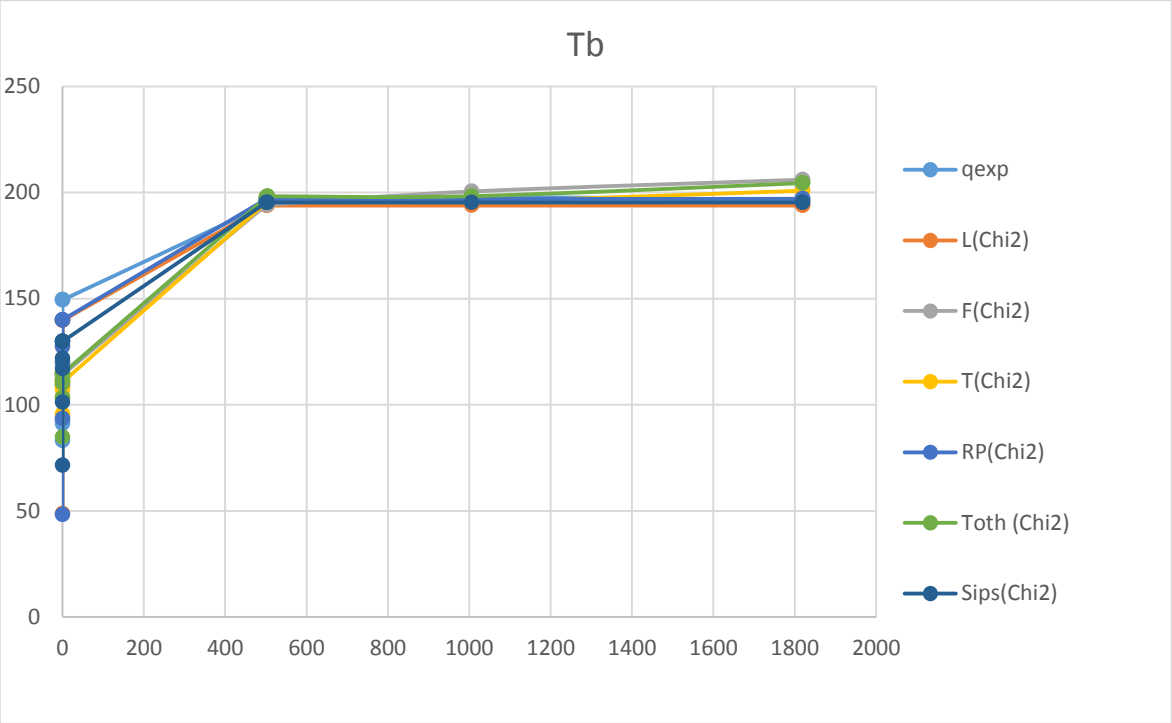

Figure 18 – Adsorption isotherms for Tb(III) uptake by the adsorbent N10O, fitted via Chi2 error function.[1]

The assessment of goodness-of-fit of the isotherms related to Tb adsorption on the BP is done using SNE. Results of calculation are collected in the Table 9. From the SNE values it can be said that Sips isotherm is again the most appropriate for predicting adsorption behavior. Overall, three-parameter isotherms describe the system better than the two-parameter.

1 - For experimental conditions, refer to the Section 6.5

Table 10 - Errors and normalized errors for adsorption isotherms under review for Tb adsorption. Fitting of experimental data is made by Chi2 objective function.[1]

	L	F	T	RP	Toth	Sips
	Chi2	Chi2	Chi2	Chi2	Chi2	Chi2
R2	0.90	0.83	0.82	0.90	0.84	0.91
chi2	27.92	38.58	36.78	28.27	31.00	18.92
RMSE	16.22	22.37	21.67	12.17	20.99	14.21
ARE	9.81	12.45	10.25	5.88	10.46	8.37
Sre	17.15	23.65	20.92	12.68	21.36	15.12
MPSD	17.47	17.82	15.73	13.49	15.88	13.09
ERRSQ	2629.41	5002.05	5166.21	2665.97	4405.49	2219.69
normalized errors						
R2	0.99	0.91	0.90	0.98	0.92	1.00
chi2	0.72	1.00	0.95	0.73	0.80	0.49
RMSE	0.73	1.00	0.97	0.54	0.94	0.64
ARE	0.79	1.00	0.82	0.47	0.84	0.67
Sre	0.73	1.00	0.88	0.54	0.90	0.64
MPSD	0.98	1.00	0.88	0.76	0.89	0.73
ERRSQ	0.51	0.97	1.00	0.52	0.85	0.43
SNE	5.44	6.88	6.41	4.54	6.15	4.60

7.6 Selectivity coefficient

Separation factors between Nd, Eu, Tb for different pH in 1M HCl medium are shown in the Figures 19 and 20. On the plots it is well seen that the separation factors are not high: on average, 1 for Tb; 1,2 for Eu; 2 for Nd. There are occasional high values but they appear by certain pH, so are not likely to become useful in real technological process. For comparison, simple Dowex ion exchange resin has separation factors between adjacent rare-earths varying from 1 to 2.6.

1 - For experimental conditions, refer to the Section 6.5

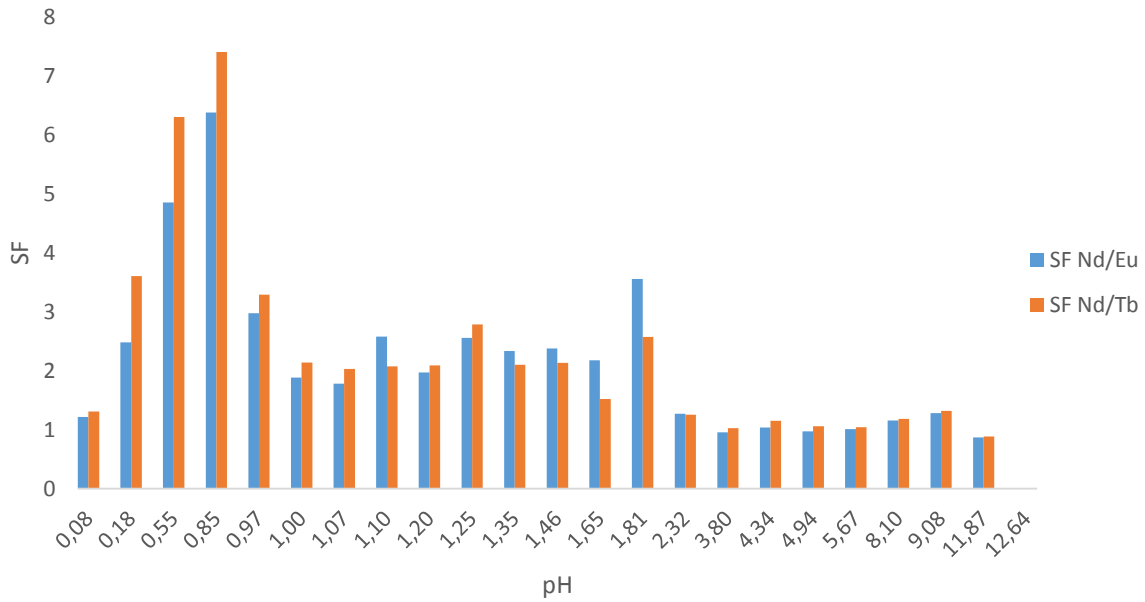

Figure 19 – Selectivity coefficients for separating Nd from Eu and Tb in aqueous solutions[1].

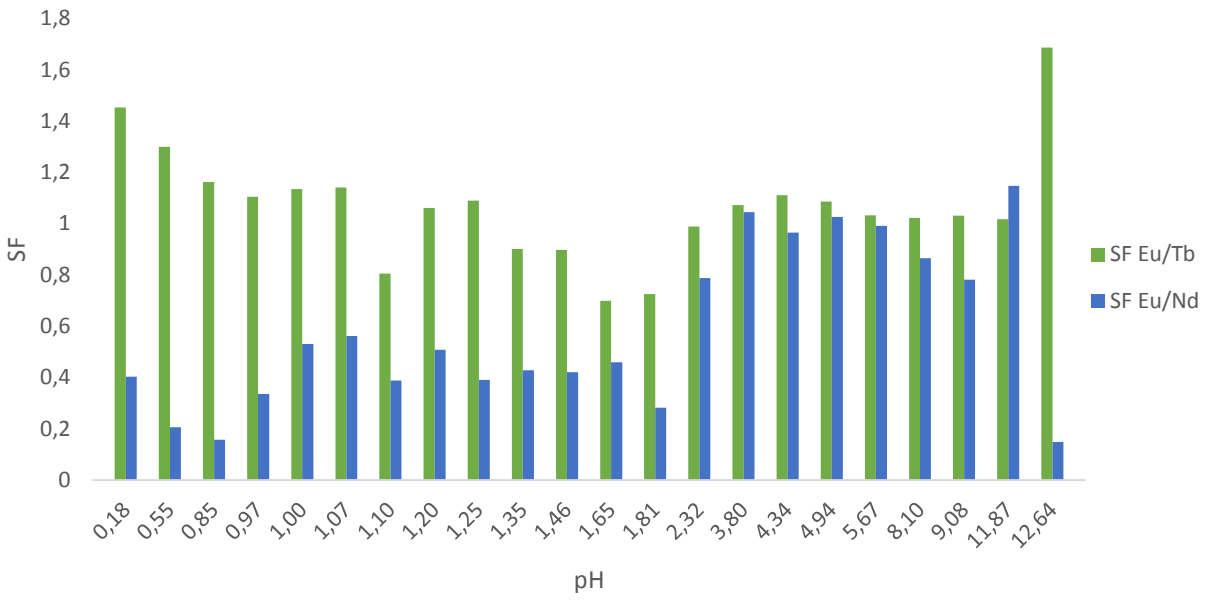

Figure 20 – Selectivity coefficients for separating Eu from Nd and Tb in aqueous solutions[1].

1 - For experimental conditions, refer to the Section 6.2

7.7 Ionic strength dependence

Adsorption dependence on ionic strength of solutions is presented on the Figures 21-23. Although there is data scattering, it can be seen that ionic strength does not have significant effect on adsorption.

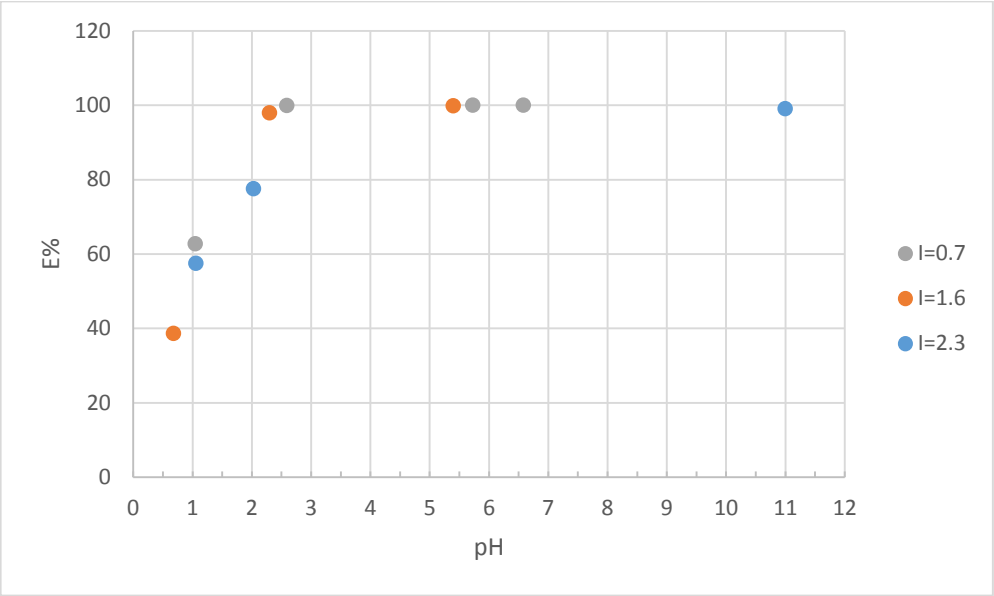

Figure 21 – Extraction percent as function of pH for three different values of ionic strength for Nd adsorption by N10O[1]

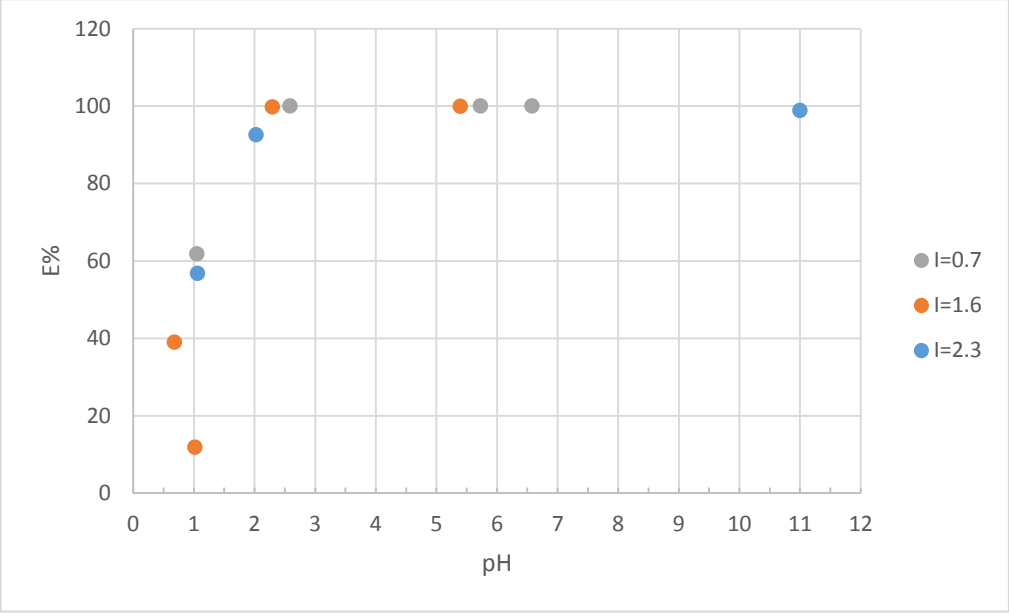

Figure 22 – Extraction percent as function of pH for three different values of ionic strength for Nd adsorption by N10O[1]

1 - For experimental conditions, refer to the Section 6.6

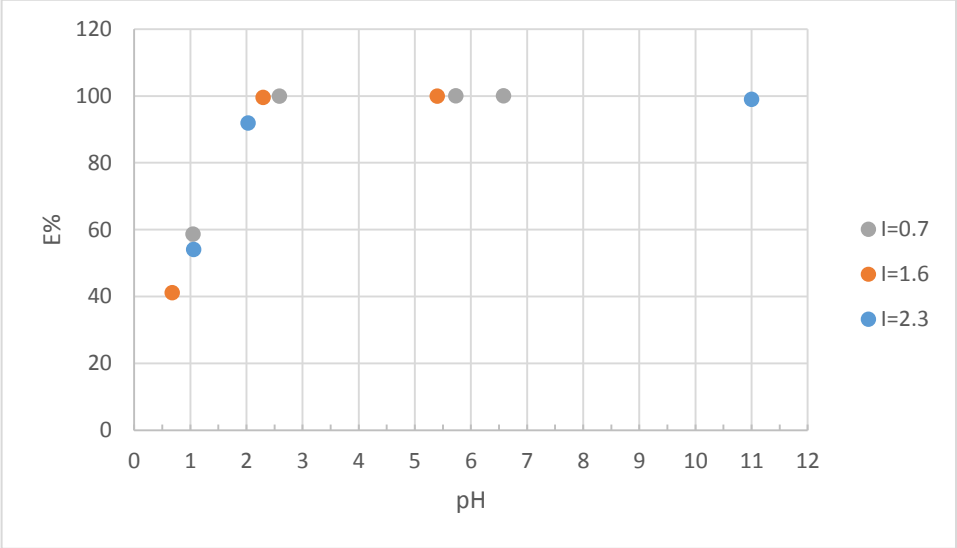

Figure 23 – Extraction percent as function of pH for three different values of ionic strength for Tb adsorption by N10O[1]

7.8 Solubility issue

During the pH-dependence experiment, a very interesting point was noted. The pH range taken into consideration was considerably wider than that covered by research group of University of Eastern Finland. Each sample received the same amount of N10O powder. The photographed result can be seen on the Figure 24. According to the report of UEF (Turhanen et al. 2015), at pH=11 solubility of N10O is less than 1 g/l. This does not agree with the evidence on the photo, which suggests values 10 times bigger. Obvious is the necessity of more precise experiments.

Figure 24 – Test-tubes with pH changing from 0 to 14. Liquid volume: 10 ml. BP amount: 0.2 g. pH in #9 is 11 and increases up to 14 in-#12.

1 - For experimental conditions, refer to the Section 6.6

8. CONCLUSIONS

As it was stated in the beginning of this paper, the main aims of the work were to test recently synthesized adsorbent and obtain the answer about its applicability for rare earth metal adsorption. Another research question was to establish optimal process parameters. Various conditions for batch adsorption were tested, namely pH, temperature, time, ionic strength. Experimental results were further processed by fitting to existing adsorption models.

It turned out that the process of adsorption was slow, 90% REM uptake was achieved only after 6 hours. This data does not comply with the data provided by University of Eastern Finland, who created and first tested the N10O adsorbent. The previous results showed very fast adsorption rate, <10 min or even faster than 1 min. Such a big disparity in kinetic results can be explained by difference in experimental conditions. Prior to applying N10O for pilot plant, checking the kinetic performance in various conditions (pH, temperature, phase ratio) would be beneficial. It was found in this research, that increased temperature enhances adsorption, 40 °C being the optimum.

Reaction and diffusion kinetic models were fitted to experimental data points by non-linear regression. Pseudo-I-order model exerted the best fit, which indicated that the adsorption reaction is of the first order. The fit for pseudo-II-order was just slightly worse, whereas Elovich equation did not suit for adsorption system. Among diffusion models, Boyd and Weber-Morris equations were fitted to experimental data by non-linear regression. The results showed that liquid film diffusion with particle diffusion control the rate of adsorption process.

The pH range for adsorption of rare earth metals by the bisphosphonate N10O is wide: 50% of the REM are adsorbed already at pH 1.5. After pH=2, total adsorption is achieved for HCl and HNO_3. For H_2SO_4, 100% extraction occurs after pH=2.5. Therefore working range resembles to the one that Cu(II) exerted (Alanne 2014). Solubility of the adsorbent turned out to be insignificantly small in acidic and basic pH. However, in very basic pH region N10O is completely dissolved in amount 0.2 g per 10 ml, leading to solubility about which is equal to 20 g/l. The right end of the pH scale was not tested previously. It is clear

that such alkaline solutions do not occur in the industry, but it would be interesting to see the full solubility plot of N10O.

The capacities of the N10O towards REM under review was high: for Nd(III) – 225 mg/g, for Eu(III) – 200 mg/g, for Tb(III) – 250 mg/g. Compared to the low-cost adsorbents studied in the last 3 years, only for Nd(III) other materials could compete with the N10O. Wang et al. (2014) states the capacity of calcium alginate as 238 mg/g, and magnetic nano-hydroxyapatite can incorporate 323 mg/g of Nd ions (Gok 2014). For Eu(III) and Tb(III) adsorption capacities are unsurpassed. The data on capacities of common ion exchange resins towards REM is not satisfying. To be able to compare the information on capacity, similar experiments should be conducted with N10O anf IX resin. Dry capacity of BP-based resins Dipex and Diphonix, is 50 mg/g and 250 mg/g correspondingly. Therefore, it can be assumed with confidence that the capacity of the N10O lies in the range of that for common ion exchangers. Selectivity coefficients lying in the range 1-2 are also comparable to commonly used materials.

Even though the capacity of N10O is high enough and selectivity coefficients are satisfying, there is one major difficulty before technological application of the adsorbent in question might be suggested: the powdered form of the sorbent. For successful application in pilot-plant or full industrial scale, N10O should be impregnated to resin beads, e.g. based on silica or calcium alginate.

During modelling of adsorption isotherms, the issue of choosing an appropriate error function came to the forefront. Indeed, this choice of one or another error function leads to drastically different results due to varying of data points weighing. The decision was made to use a summarized error function for initial assessment of error function performance. This method can be considered more reliable, because it takes into account several error functions, thus averages the deviations. However, the main thing in considering error method is to have even distribution of experimental data points without big scattering. In general, Chi2 turned out to be the best function for fitting empiric loading isotherms. Langmuir model showed the best fit among the 2-parameter isotherm models. It was even comparable with three-parameter isotherms, which matched the data much better than two-parameter. The best fit was found for Sips (Langmuir-Freundlich isotherm).

To sum it up, N10O is a promising material for selective adsorption of rare earth ions due to high capacity, decent selectivity. However, further research is needed to create industrially applicable version of N10O. The future research should also study solubility of N10O adsorbent, as well as kinetics in non-ideal conditions.

9. REFERENCES

Akkaya R. 2014. Terbium adsorption onto polyhydroxyethylmethacrylate–hydroxyapatite composite and its modified composition by phytic acid. Desalination and Water Treatment, 52:7-9, 1440-1447. DOI: 10.1080/19443994.2013.793922

Alanne A. 2014. Novel Applications Related to Bisphosphorus Compounds. University of Eastern Finland, Faculty of Health Sciences. Publications of the University of Eastern Finland, dissertations in Health Sciences, 212.

Albadarin A., Al-Muhtaseb A., Al-laqtah N., Walker S., Allen J., Ahmad M. 2011. Biosorption of toxic chromium from aqueous phase by lignin: mechanism, effect of other metal ions and salts. Chemical Engineering Journal 169 (2011).

Alonso E., Sherman A. 2012. Evaluating rare earth element availability: A case with revolutionary demand from clean technologies. Environmental science and technology, 46.

Anastopoulos I. et al. 2016. Adsorption of rare earth metals: A review of recent literature. Journal of Molecular Liquids, 221 (2016).

Arabieh M., Khodabandeh M., Karimi-Jafari M., Platas-Iglesias L., Zare K. 2015. Complexation of Sm^{3+} and pamidronate: A DFT study. Journal of rare earths, vol. 33:3.

Azizian S. 2004. Kinetic models of sorption: a theoretical analysis. 2004. Journal of Colloid and Interface Science, 276.

Beauford R. 2010. Rare earth elements, 2010 summary. [online document] Available from: http://rareearthelements.us/ [Accessed 1 August 2016].

Binnemans K., Jones P., Blanpain B., Van Gerven T., Yang Y., Walton A., Buchert M. 2013. Recycling of rare earths: a critical review. Journal of Cleaner Production 51.

Bruce D., Hietbrink B., Dubois K. 1963. The acute mammalian toxicity of rare earth nitrates and oxides. Toxicol. Appl. Pharmacol., 5:750-9.

Butnariu M, Negrea P. et al. 2015 Remediation of rare earth element pollutants by sorption process using organic natural sorbents. Int. J. Environ. Res. Public Health, 12 (2015).

Cadogan C., Lee, S. et al. 2014. Efficiencies of chitosan nanoparticles and crab shell particles in europium uptake from aqueous solutions through biosorption: synthesis and characterization, Int. Biodeterior. Biodegrad., 95.

Chiarizia R., Horwitz E.P., Alexandrators S.D. & Gula M.J. 1997. Diphonix® resin: a review of its properties and applications. Separation Science and Technology, vol. 32.

Chiarizia R., McAlister D.R. & Herlinger A.W. 2001. Solvent extraction by dialkylsubstituted diphosphonic acids in a depolymerizing diluent. II. Fe(III) and actidine ions. Solvent Extraction and Ion Exchange, vol. 19, no. 3.

CRM_Innonet. 2016. Critical Raw Materials Innovation Network – Towards an integrated community driving innovation in the field of critical raw material substitution for the benefit of EU industry. [online document] Available at: http://cordis.europa.eu/result/rcn/176863_en.html [Accessed 28 May 2016].

Das N. and Das D. 2013. Recovery of rare earth metals through biosorption: an overview. Journal of Rare Earths, vol. 31:10. DOI:10.1016/S1002-0721(13)60009-5

Deng S., Zhang G., Yang L. 2016. Facile preparation of amidoxime-functionalized fiber by microwave-assisted method for the enhanced adsorption of chromium(VI) from aqueous solution. RSC Advances, 6.

Diniz V. and Volesky A. 2005. Biosorption of La, Eu and Yb using Sargassum biomass. Water Res., 39 (2005).

Dolatyari L, Yaftian M., Rostamnia S. 2016. Adsorption characteristics of Eu(III) and Th(IV) ions onto modified mesoporous silica SBA-15 materials. 2016. Journal of the Taiwan Institute of Chemical Engineers, vol. 60. DOI: 10.1016/j.jtice.2015.11.004

ERECON. 2015. Strengthening the European rare earths supply chain: Challenges and policy options. Kooroshy, J., G. Tiess, A. Tukker, and A. Walton (eds.). [online document] Available at: http://ec.europa.eu/growth/sectors/raw-materials/specific-interest/erecon/index_en.htm [Accessed 28 May 2016].

Fierro V., Torne-Fernandez V., Montane D., Celzard A. 2007. Adsorption of phenol onto activated carbons having different textural and surface properties. Microporous and Mesoporous Materials, 111 (2008).

Foo K.Y., Hameed B.H. 2009. Insights into the modeling of adsorption isotherm systems. Chemical Engineering Journal, 156 (2010). DOI:10.1016/j.cej.2009.09.013

Galhoum M.G., Mafhouz S.T., Abdel-Rehem N.A. 2015. Cysteine-functionalized chitosan magnetic nano-based particles for the recovery of light and heavy rare earth metals: uptake kinetics and sorption isotherms. Nanomaterials, 5 (2015).

Ghosh S., Chan J.M.W., Lea C.R. 2004. Effects of bisphosphonates on the growth of Entamoeba histolytica and Plasmodium species in vitro and in vivo. Journal of Medicinal Chemistry, vol. 47, no. 1.

Giles C. H., Macewan T.H., Nalkhwa S.N., Smith D. 1960. Studies in adsorption. XI. A system of classification of solution adsorption isotherms, etc. J. Chem. Soc. 20:2.
Gimurtu A. and Lifton J. 2012. The Only Five Rare Earth Elements that Matter: Jack Lifton. The Critical Metals Report [online document] Available at: https://www.streetwisereports.com/pub/na/the-only-five-rare-earth-elements-that-matter-jack-lifton [Accessed 1 June 2016].

Gładysz-Płaska M., Majdan, E., Grabias V. 2014. Adsorption of La, Eu and Lu on raw and modified red clay. J. Radioanal. Nucl. Chem., 301.

Gnant M. & Clézardin P. 2012, Direct and indirect anticancer activity of bisphosphonates: A brief review of published literature. Cancer Treatment Reviews, vol. 38, no. 5.

Gok C. 2014. Neodymium and samarium recovery by magnetic nano-hydroxyapatite. Journal of Rare Earths**,** vol. 26:2.

Granados-Correa F. et al. 2013. Adsorption behaviour of La (III) and Eu (III) ions from aqueous solutions by hydroxyapatite: kinetic, isotherm, and thermodynamic studies. J. Chem. (2013), 1–9.

Gumienna-Kontecka E., Jezierska J. 2002a. Bisphosphonate chelating agents: Coordination ability of 1-phenyl-1-hydroxymethylene bisphosphonate towards Cu2+ ions. Journal of Inorganic Biochemistry, vol. 89, no. 1.

Gumienna-Kontecka E., Silvagni R., Lipinski R. 2002b. Bisphosphonate chelating agents: complexation of Fe(III) and Al(III) by 1-phenyl-1-hydroxymethylene bisphosphonate and its analogues. Inorganica Chimica Acta, vol. 339.

Guo Z., Li Y. et al. 2015. Fabrication of Fe3O4@ cyclodextrin magnetic composite for REE adsorption. Adv. Mater., 29.

Gupta C . K . and Krishnamurthy N. 2004. Extractive Metallurgy of Rare Earths. Boca Raton: CRC Press. [online document] Available from: http://vector.umd.edu/images/links/ Extractive_Metallurgy_of_Rare_Earths_Gupta.pdf. [Accessed 21 August 2016].

Gutfleisch O., Willard M.A.et al. 2011. Magnetic materials and devices for the 21st century: stronger, lighter, and more energy efficient. Adv. Mater., 23.

Haerifar M., Azizian S. 2013. Mixed Surface Reaction and Diffusion-Controlled Kinetic Model for Adsorption at the Solid/Solution Interface. J. Phys. Chem., 117. DOI: 10.1021/jp401571m.

Hameed B., El-Khaiary M.. 2008. Batch removal of malachite green from aqueous solutions by adsorption on oil palm trunk fibre: equilibrium isotherms and kinetic studies, J. Hazard. Mater. 154.

Haynes W. 2009. CRC handbook of chemistry and physics: a ready-reference book of chemical and physical data. Boca Raton, CRC Press.

Herlinger A.W., Ferraro J.R., Chiarizia R. & Horwitz E.P. 1997. An investigation of P, P′-di(2-ethylhexyl) methane diphosphonic acid and some of its metal complexes. Polyhedron, vol. 16, no. 11.

Ho Y., McKay G. 1998. Comparison of chemisorption kinetic models applied to pollutant removal on various sorbents. Institution of Chemical Engineers, Trans IChemE, Vol 76, Part B.

Horwitz E.P., Chiarizia R. & Dietz M.L. 1997. DIPEX: A new extraction chromatographic material for the separation and preconcentration of actinides from aqueous solution. Reactive and Functional Polymers, vol. 33, no. 1.

Humpfries M. 2013. Rare earth elements: The global supply chain. Congressional Research Service, December 16, 2013.

Iannitti T., Rosini S., Lodi D. 2012. Bisphosphonates: focus on inflammation and bone loss. American Journal of Therapeutics, vol. 19, no. 3.

Kolodynska D., Hubicki Z. 2012. Investigation of Sorption and Separation of Lanthanides on the Ion Exchangers of Various Types. Ion exchange technologies, Chapter 6. ISBN: 978-953-51-0836-8. DOI: 10.5772/50857

Kumar S., Senthamarai N. et al. 2014. Adsorption kinetics, mechanism, isotherm, and thermodynamic analysis of copper ions onto the surface modified agricultural waste. Environ. Prog. Sustainable Energy, 33: 28–37. DOI:10.1002/ep.11741

Kunnas-Hiltunen S., Laurila E. et al. 2010. Organic-inorganic hybrid materials: Syntheses, X-ray diffraction study, and characterisations of manganese, cobalt, and copper complexes of modified bis(phosphonates). Zeitschrift Für Anorganische Und Allgemeine Chemie, vol. 636, no. 5.

Largitte L., Pasquier R. 2016. A review of the kinetics adsorption models and their application to the adsorption of lead by an activated carbon. IChemE 109. DOI: 10.1016/j.cherd.2016.02.006

Lin J. and Wang L. 2009. Comparison between linear and non-linear forms of pseudo-first-order and pseudo-second-order adsorption kinetic models for the removal of methylene blue by activated carbon. Frontiers of Environmental Science & Engineering in China, September 2009, Volume 3, Issue 3. DOI:10.1007/s11783-009-0030-7

Lohse D.L. and Sevov S.C. 1997. $CO_2(O_3P\text{-}CH_2\text{-}PO_3)\cdot H_2O$: A Novel microporous diphosphonate with an inorganic framework and hydrocarbon-lined hydrophobic channels. Angewandte Chemie International Edition in English, vol. 36, no. 15.

Luca V., Hanna J. 2015. A versatile Zr(IV)-organophosphonate coordination polymer platform for the selective adsorption of lanthanides and actinides. Hydrometallurgy, vol. 154.

Matczak-Jon E., Kowalik-Jankowska T. 2010. Specificity of the zinc(II), magnesium(II) and calcium(II) complexation by (pyridin-2-yl) aminomethane-1,1-diphosphonic acids and related 1,3-(thiazol-2-yl) and 1,3-(benzothiazol-2-yl) derivatives. Dalton Transactions, vol. 39, no. 5.

Matveev S.V., Bel'skii F.I. et al. 1998. N-Substituted 2-aminoethylidenediphosphonic acids as complexones. Russian Chemical Bulletin, vol. 47, no. 9.

Moeller T. and Kremers H.E. 1945. On characteristics of lanthanides. Chem. Rev., 37.

Morgan G. and Lipton A. 2010. Antitumor effects and anticancer applications of bisphosphonates. Seminars in Oncology, vol. 37, Suppl 2.

Naser A., El-deen G. et al. 2015. Elaboration of impregnated composite for sorption of europium and neodymium ions from aqueous solutions. J. Ind. Eng. Chem., 32 (2015).

Nash K.L. 1997. F-Element complexation by diphosphonate ligands. Journal of Alloys and Compounds, vol. 249, no. 1–2.

Neff G.A., Helfrich M.R., Clifton M.C. & Page C.J. 2000. Layer-by-layer growth of acentric multilayers of Zr and azobenzene bis (phosphonate): Structure, composition, and second-order nonlinear optical properties. Chemistry of Materials, vol. 12, no. 8.

Okewale A., Babayemi K., Olalekan A.P. Adsorption Isotherms and Kinetics Models of Starchy Adsorbents on Uptake of Water from Ethanol – Water Systems. 2013. International Journal of Applied Science and Technology Vol. 3 No. 1.

Ogata T. et al. 2013. Adsorption behavior of rare earth elements on silica gel modified with diglycol amic acid Hydrometallurgy, 152 (2015).

Ogata T. et al. 2013. Selective recovery of heavy rare earth elements from apatite with an adsorbent bearing immobilized tridentate amido ligands. Hydrometallurgy, 150 (2013).

Ogata T. et al. 2013. Selective recovery of heavy rare earth elements from apatite with an adsorbent bearing immobilized tridentate amido ligands. Sep. Purif. Technol., 159 (2016).

Prodromou M., Pashalidis I. 2016. Europium adsorption by non-treated and chemically
Purolite C150TLH Information brochure [online document]. [Accessed 01.08.2016]. Available at: http://www.purolite.com/RelId/619248/isvars/default/strong_acid_cation
_macroporous.htm

Qiu H., Lv L., Pan B. et al. 2009. Critical review in adsorption kinetic models. Sci. A., 10: 716. DOI:10.1631/jzus.A0820524

Raji F., Saraeian A., Pakizeha M., Attarzadeh F. 2015. Removal of Pb(II) from aqueous solution by mesoporous silica MCM-41 modified by ZnCl2: kinetics, thermodynamics, and isotherms. RSC Adv., 5, 37066. DOI: 10.1039/c5ra01192b

Redlich O. and Peterson D.L. 1959. A Useful Adsorption Isotherm. The Journal of Physical Chemistry 63 (6).

Reddy N., Rao K. et al. 2016. Synthesis of 1-acryloyl-3-phenyl thiourea based pH sensitive hydrogels for removal of samarium and terbium. Macromol. Res., 24: 494. DOI:10.1007/s13233-016-4068-7

Roosen J., Binnemans K. 2014. Adsorption and chromatographic separation of rare earths with EDTA- and DTPA-functionalized chitosan biopolymers. Journal of Materials Chemistry, A2.

Roosen J., Binnemans K. et al. 2015. Shaping of alginate–silica hybrid materials into microspheres through vibrating-nozzle technology and their use for the recovery of neodymium from aqueous solutions. Ind. Eng. Chem. Res., 54 (2015).

Sainio T. 2015. Chemical separation methods. BJ02A3020 course lecture notes. Lappeenranta. 2015/2016 study year. Lappeenranta University of Technology.

Sawicki M., Lecercle D., Grillon G. et al. 2008. Bisphosphonate sequestering agents. Synthesis and preliminary evaluation for in vitro and in vivo uranium(VI) chelation. European Journal of Medicinal Chemistry, vol. 43, no. 12.

Shubert J. 1949. Applications of Ion exchange to the separation of inorganic cations. In: F. Nachod, ed., Ion Exchange: Theory and Application. New York, Academic Press. ISBN: 978-0-12-395613-2

SUC Report. 2014. Commodities at a glance - special issue on rare earths. United Nations Conference on Trade and Development (UNCTAD) 5, New York and Geneva. [online document] Available at: http://unctad.org/en/PublicationsLibrary/suc2014d1_en.pdf [Accessed 21 June 2016].

Svard M. 2015. Research topic for School of Chemical Science and Engineering of KTH. Stockholm, Sweden. [online document] Available at: https://www.kth.se/en/che/divisions/transport_phenomena/research/ree/separation-of-rare-earth-metals-1.376342 [Accessed 02 August 2016].

Terry M. 2011. Rare Earths - A Brief Summary and Focus Elements - Seeking Alpha. [online document] Available from http://seekingalpha.com/article/244792-rare-earths-a-brief-summary-and-focus-elements [Accessed 23 July 2016].

Tompkins F.C. 1978. Chemisorption of gases on metals. London: Academic Press.

Topp N.E. 1964. Modern techniques for separating the rare-earth elements. Less-Common Metals 7 (1964).

Turhanen A., Vepsalainen J., Peraniemi S. 2015. Advanced material and approach for metal ions removal from aqueous solutions. Scientific reports, 5:8992. DOI: 10.1038/srep08992

U.S. Geological Survey. 2016. Mineral Commodity Summaries. Reston: National Minerals Infromation Center. [online] Available at http://pubs.er.usgs.gov/publication/70170140 [Accessed 13 July 2016]

Vasylechko V. et al. 2015. A solid-phase extraction method using Transcarpathian clinoptilolite for preconcentration of trace amounts of terbium in water samples. Chemistry Central Journal, 9:45. DOI: 10.1186/s13065-015-0118-z

Virolainen S. 2016. Hydrometallurgy lecture notes. BJ02A3050 Hydrometallurgy course, Lappeenranta, 2015/2016 study year. Lappeenranta University of Technology.

Wang X., Zhao H., Wei X et al. 2014. Adsorption of rare earths (III) by calcium alginate–poly glutamic acid hybrid gels. J. Chem. Technol. Biotechnol., 89 (2014).

Wedepohl H. 1995. The composition of the continental crust. Geochimica et Cosmochimica Acta, Vol. 59, No. 7.

Wharmby M.T., Mowat J.P., Thompson S.P. & Wright P.A. 2011. Extending the pore size of crystalline metal phosphonates toward the mesoporous regime by isoreticular synthesis. Journal of the American Chemical Society, vol. 133, no. 5.

Xiaoqi S et al. 2016. Adsorption of rare earth ions using carbonized polydopamine nano carbon shells. J. Rare Earths, 34.

Xie F., Zhang T., Dreisinger D., Doyle F. 2014. A critical review on solvent extraction of rare earths from aqueous solutions. Minerals Engineering, vol. 56, pp. 10-28.

Yao T., Xiao Y., Wu X. et al. 2016. Adsorption of Eu (III) on sulfonated graphene oxide: combined macroscopic and modeling techniques. J. Mol. Liq., 215 (2016),.

Yin P., Xu M., Qu R. et al. 2013. Uptake of gold(III) from waste gold solution onto biomass-based adsorbents organophosphonic acid functionalized spent buckwheat hulls. Bioresource Technology, vol. 128.

Zhang J., Zhao B., Schreiner B. 2016. Separation hydrometallurgy of rare earth elements. Springer. ISBN 978-3-319-28235-0.

Zhao F., Repo E., Sillanpää M. 2015. An EDTA-β-cyclodextrin material for the adsorption of rare earth elements and its application in preconcentration of rare earth elements in seawater. J. Colloid Interface Sci., 465.

Zhu Y., Zheng Y. 2015. A simple approach to fabricate granular adsorbent for adsorption of rare elements. Int. J. Biol. Macromol., 72.